Improving filmogenic and barrier properties of nanocellulose films by addition of biodegradable plasticizers

Julia Fernández-Santos[1], Cristina Valls[2], Oriol Cusola[3], M. Blanca Roncero[4]

[1,2,3,4] CELBIOTECH_Paper Engineering Research Group, Universitat Politècnica de Catalunya_BarcelonaTech, 08222 Terrassa, Spain

Correspondence to: M. Blanca Roncero (E-mail: blanca.roncero@upc.edu / telephone: 0034 93 7398210)

Julia Fernández-Santos: ORCID 0000-0002-9105-9117 (julia.fernandez.santos@upc.edu)

Cristina Valls: ORCID 0000-0003-2307-1779 (cristina.valls@upc.edu)

Oriol Cusola: ORCID 0000-0002-1407-8285 (oriol.cusola@upc.edu)

M. Blanca Roncero: ORCID 0000-0002-2694-2368 (blanca.roncero@upc.edu)

ABSTRACT

Cellulose nanocrystals (CNC) were mixed with various additives to obtain films with good barrier and mechanical properties as replacements for petroleum-based plastics. The influence of different doses of additives including glycerol, maltitol, xylitol, mannitol, gellan gum and ethylene glycol on the resulting films was examined. Both the type of additive and its amount were found to affect film morphology, barrier, optical and mechanical properties. Most of the additives showed good results at low doses. All additives, except ethylene glycol and mannitol, improved film elongation; also, they increased tensile strength, and decreased air and water permeance. The films containing sorbitol, xylitol and maltitol exhibited the highest barrier properties, providing films with totally resistance to oxygen under 60% of RH conditions. Interestingly, those films containing additives were more easily biodegraded than the control film.

Keywords

Cellulose nanocrystals, additives, cellulose-based films, barrier properties and biodegradability.

Synopsis sentence

Studying different additives to improve the mechanical, optical and barrier properties of CNC-based films for several applications.

Abbreviations

CNC: Cellulose nanocrystals

CNF: cellulose nanofibers

Sor: sorbitol

Gly: glycerol

Mal: maltitol

Xyl: xylitol

Man: mannitol

Gg: gellan gum

Eg: ethylene glycol

INTRODUCTION

Quality of life is increasingly been associated with the development of innovative, sustainable products obtained with more efficient procedures using renewable, sustainable resources [1]. Petroleum-based plastics are posing great challenges to health and the environment across the world. Developing effective alternatives is a current focus of much research in various scientific disciplines. For example, plastics are the basis for food packaging and the sources of severe health and environmental problems as a result [2]. The increasing concern with food safety and preservation of the environment has promoted the development of various types of biopolymers as non-toxic, biodegradable alternatives of greater quality and without waste disposal problems [3].

Cellulose, which possesses a highly crystalline or fibrillar structure, is one of the most abundant natural biopolymers. This has boosted production of new, cellulose-based ecological packaging materials. However, the hydrophilic nature and porous structure of the most common cellulose products (e.g., cardboard) restricts some potential uses [4]. Nanotechnology has lately emerged as one of the most promising tools for developing new materials. For example, cellulose can be converted into cellulose nanofibers (CNF) and cellulose nanocrystals (CNC), two different types of biomaterials with highly interesting properties [5].

Cellulose nanocrystals can be obtained from various sources including cotton, cotton linters, kenaf fibre, wheat straw and wood fibre [5,6]. The process involves hydrolysis, usually with sulphuric acid, of the amorphous portion, giving rise to crystalline cellulose nanostructures [1,7]. The properties of cellulose nanocrystals and the yields in which their derivatives are obtained depend on various factors including the particular raw material and production methods used [8], any pretreatment of the cellulose source [9] and whether the CNC suspension is post-treated [10].

Cellulose nanocrystals possesses a number of desirable mechanical and chemical properties including a high tensile strength and rigidity, also a large number of surface hydroxyl groups [11] and a high surface area due

to the dimensional structure of CNC, allowing a strong interaction with other matrices to form nanocomposites [12]. This has promoted research into the production and characterization of films obtained from CNC suspensions [13,14].

Cellulose nanocrystals can thus be an effective choice for advantageously circumventing some problems of porous packaging materials. However, its limited ability to form three-dimensional networks can restrict their use for obtaining versatile materials (Aulin, Gällstedt, & Lindström, 2010; Herrera et al., 2017). CNC films are highly rigid and brittle, and hence difficult to handle. These shortcomings have been addressed by previously mixing CNC with a plasticizer, the most common being sorbitol and glycerol [4,5,16–18]. The surface of cellulose nanocrystals contains easily accessed hydroxyl groups that may interact with those in plasticizers, thereby altering the morphology of the crystals and conferring them new properties [5]. However, it remains unclear which is the most suitable additive and its dose to be used as plasticizer in order to improve the film formation of CNC and its mechanical and barrier properties, and also, how plasticizers affect the structure of CNC films. In this study, we compared the effects of various additives on the properties of CNC films with a view to identifying the proper amount and type of plasticizer that is more compatible with nanocellulose. Plasticizers are low molecular weight compounds that are added to the polymer matrix to improve the film flexibility and workability. There is a wide range of plasticizers [4,5,16,18–31], but their effectiveness will depend on the type of polymer network, which in our case will be nanocellulose. In order to achieve good compatibility with nanocellulose seven additives, namely: sorbitol (Sor), glycerol (Gly), maltitol (Mal), xylitol (Xyl), mannitol (Man), gellan gum (Gg) and ethylene glycol (Eg) were selected and tested in CNC-based films. These plasticizers have a structure similar to nanocellulose, with free hydroxyl groups, making them more compatible to join with nanocellulose and form a homogeneous film. The resulting films with different amount of additives were characterized in terms of strength, visual appearance, barrier properties, crystallinity, morphology and biodegradability.

The purpose is to establish the most suitable plasticizer to be used in CNC-based films depending on the required film property. To our knowledge, the study and comparison of all these additives in CNC-based films and their biodegradability characterization has not been previously reported.

MATERIALS AND METHODS

Materials

Cellulose nanocrystals, provided by University of Maine (Maine, United States), were used as main raw material. The cellulose nanocrystals were derived from wood pulp and had dimensions of approximately 5

nanometers (nm) in diameter and 150-200 nanometers in length. A 3% suspension was used in our tests. The plasticizers used were: sorbitol, maltitol, xylitol and mannitol from Acros Organics BVBA (Geel, Belgium), glycerol and ethylene glycol from Panreac Quimica Sau (Barcelona, Spain) and gellan gum, Gelzan TM, from Sigma-Aldrich S.A. (Madrid, Spain). Additional information about the additives is shown in supporting information (Table S1).

Preparation of CNC-based films by casting method

13.8 grams of CNC (12.1% wt) were deposited on a polystyrene plastic plate (100 cm^2) and allowed to evaporate at controlled humidity (50% RH) and temperature (23°C) conditions, for about 5 days. The film obtained without the addition of any additive, was the control film used throughout this study.

In order to overcome the brittle nature of CNC films, plasticizers such as sorbitol, glycerol, maltitol, xylitol, mannitol, gellan gum and ethylene glycol were used and applied in different percentages (10, 15, 20, 25%) of the dry weight of CNCs. For accurate homogenization, the mixture was stirred with vigorously shaking for one hour.

Characterization of CNC-based films

Optical properties

The light absorption was measured at room temperature in steps of 1nm, in the range of 200 to 900 nm with an Evolution 600 UV-visible spectrophotometer. Transmittance of the film at 600 nm was also measured. Specular gloss was measured following the standard ISO 8254-3. The transparency of the films was calculated from the percent transmittance of light at 600 nm, following the equation 1 [32]:

$$Transparency = \left(\frac{log\%T600}{x}\right) \quad (1)$$

Where %T600 is the percent transmittance at 600 nm and x is the film thickness (mm).

A minimum of five replicates were tested for each film sample and the average values were represented.

Mechanical properties

Mechanical properties of the films such as tensile strength, elongation at break and Young's modulus were carried out by using a Metrotec-quality control instruments T5K equipped with a 500N load cell. The loading

speed was 10 mm/min. The films were cut into rectangular shape with 15mm width. A minimum of ten replicates were tested for each film sample and the average values were represented.

Structural properties

Thickness, basis weight and density were measured according to ISO 534:2011.

Porosity is the ratio of pore volume (void volume) to total volume. In this way, theoretical porosity can be calculated according to the equation 2 [5]. Theoretical density was calculated from the density values of CNCs, Sor, Gly, Mal, Xyl, Man, Gg and Eg which were 1.57, 1.49, 1.26, 0.6, 1.52, 1.49, 0.8 and 1.1 g/cm^3, respectively. The measured density is the bulk density of the films, and it was calculated as the ratio between basis weight and thickness of the material (film) (ISO 534).

$$Porosity\ (\%) = \frac{(theoretical\ density - measured\ density)}{theoretical\ density} x100 \qquad (2)$$

Roughness of the films was measured following the ISO 8791-2:2013, by the air leakage Bendtsen method. It measures the air volume per minute (ml/min) which has leaked out when the film is clamped between a flat glass plate and a circular metal head.

Surface and cross sections of the films were observed by SEM (JSM 7100 F) using a LED filter. All the samples were graphite coated using EMITECH K950X221.

A minimum of five replicates were tested for each film sample and the average values were represented.

Barrier properties

Barrier properties such as resistance to air, water (water absorption and hydrophobicity), oil, oxygen and vapor were tested.

Air permeability was measured following the standard ISO 5636-3:2013, by the Bendtsen method. Water absorption (WDT-water drop test) was evaluated using the TAPPI T835, in which a drop of water is deposited on the surface of film and then it is measured the time that it took to disappear the specular gloss of the drop of water. The hydrophobicity was measured by the water contact angle (WCA). WCA measurements were made using a Dataphysics OCA15EC contact angle goniophotometer using an image capture ratio of 25 frame/s. A 4µL water drop was delivered to sample surface and at least 5 measurements were made for each sample. Oil resistance was measured in accordance with the standard ISO 16532-3:2010 (turpentine test). In this method a quantity of silica sand is placed on the film and saturated with dyed turpentine, and it is measured the time taken for the dye to penetrate the film. Oxygen permeability was measured using MOCON OX-TRAN® Model 1/50

with an atmospheric oxygen concentration of 100% at 23°C temperature and at different relative humidity (20, 40, 60 and 80%). Water vapor transmission rate of the films at 25% of plasticizer was measured according to the standard procedure ISO 2528 (2017) at 25° C and at two relative humidities, 50% and 90% RH. The procedure was carried out as follows: an aluminium cup containing $CaCl_2$ desiccant was sealed by the test film (50 cm^2 exchange film area) with paraffin wax at 90° C and placed in a climatic chamber for controlling the environmental conditions. All tests were performed in duplicate. The WVTR ($g \cdot m^{-2} \cdot day^{-1}$) was determined using the equation 3:

$$WVTR = \frac{m*24*10^4}{S*t} \quad (3)$$

where m is the increase in mass, in grams, of the assembly during the time t; S is the area in the tested surface of the test piece in cm^2 and t is the total duration, in hours, of the last two stable exposure periods.

A minimum of five replicates were tested for each film sample and the average values were represented.

Surface free energy (SFE)

The surface free energy (SFE) was evaluated using the Owens, Wendt, Rabel and Kalble (OWRK) method[33]. Briefly, several drops of deionized water, ethylene glycol and diiodomethane were applied to the surface of the samples and the corresponding contact angles were measured by Dataphysics OCA15EC contact angle goniophotometer using an image capture ratio of 25 frame/s. At least five droplets of each liquid were dispensed in different regions. The total surface free energy was computed as the sum of the polar and disperse contributions. The interfacial energy was calculated according to OWRK from the contributions of the liquid and the solid by forming the geometric mean:

$$\sigma_l(1 + cos\theta) = 2\sqrt{\sigma_l^d \sigma_s^d} + 2\sqrt{\sigma_l^p \sigma_s^p} \quad (4)^{33}$$

here, θ is the contact angle, σ_l the surface tension of the liquid, σ_l^d and σ_l^p represent the disperse and polar parts of the liquid, while σ_s^d and σ_s^p stand for the respective contributions of the solid. This gives an equation of a straight line which allows calculation of σ_s^p from the slope of the fitted line and σ_s^d from the intersection with the vertical axis. A minimum of five replicates were tested for each film sample and the average values were represented.

FTIR spectroscopy

FTIR spectra of CNC films were recorded in duplicate at room temperature using an ATR-FTIR spectrophotometer (Spectrum 100, Perkin Elmer, USA). FTIR spectral analyses were conducted within the wavenumber range of 500-4000 cm-1. A total of 64 scans were run to collect each spectrum at a 1 cm-1 resolution. The results of the spectra were normalized.

X-ray diffraction (XRD)

CNC films were subjected to X-ray diffractometry analysis (PANalytical X'Pert PRO MPD Alpha1 powder diffractometer in a Bragg-Brentano θ/2θ geometry of 240 millimetres of radius). The samples were analysed at the radiation wavelength of 1.5406 Å and 45 kV – 40 mA for the work power. Samples were scanned from 2 to 60°, 2Θ range. The samples were mounted with no support fixed by mean of two polyoxymethylene rings, and analysed in reflection geometry. The crystallinity index (CI) was calculated based on equation 5. [34].

$$\mathrm{CrI}(\%) = \frac{I_c - I_{am}}{I_c} \times 100 \qquad (5)$$

where I_c is the maximum intensity of the lattice diffraction and I_{am} is the intensity of the peak at 2Θ = 18°, which corresponds to the amorphous part of cellulose. The intensity of the peaks was measured as the maximum value obtained for the peak taking into account a baseline.

Biodegradability of CNC-additives films

In order to study the final aerobic biodegradability of the films obtained in the present study, an assay was carried out under controlled composting conditions, during a period of 90 days. The methodology of the UNE-EN ISO 17556 standard was adapted. The test method determines the total biodegradability of the degraded material. It was carried out under conditions of simulation of an intensive aerobic composting process. Ripe derivative of stabilized compost from the composting plant of the 'Parc Ambiental de Bufalvent' (Manresa, Catalonia) was used as inoculum rich in microorganisms.

The containers with the material tested were agitated weekly and a constant humidity was maintained by spraying deionized water once a week, controlling the good condition of the compost. A constant rate of CO_2-free air entered the containers and swept along CO_2 generated. The CO_2 was collected in an alkaline trap (0.05M NaOH) and the CO_2 produced is calculated from the evaluation of NaOH consumed by tritation with HCl 0.05M. After 90 days of testing, from the datum of CO_2 produced, the biodegradability of each of the tested materials was calculated.

RESULTS AND DISCUSSION

Optical properties

One of the most interesting properties of bioplastics is transparency. Nanofibrillar and cellulose nanocrystals films are usually translucent [35]. Figure S1 (A) (supplementary material) shows photographs of the orthogonal projection of CNC films (25% additive dose) and control film. A comparison with Figure S1 (B), which corresponds to an oblique projection, reveals differences in colour and specular gloss. According to Liu et al. 2017 this kind of coloration, which changes with the observing angle, is deemed structural colour.

The optical properties of CNC films can be examined from their transmittance as measured by UV–Vis spectrophotometry [usually at 600 nm, a wavelength in the middle of the visible spectral region [37]], and also from their specular gloss. Transparency values of Sor, Xyl or Man (at 10%) were higher than those of control film [Figure 1a)]. The additives leading to the lowest transparency were Gg at both 10 and 25%, and Man at 25%, also showing the lowest specular gloss values [Figure 1b)]. Murrieta-Martínez et al. 2019 also obtained low transparency when mannitol was applied as a plasticizer on squid protein in comparison with glycerol, sorbitol, maltitol, and xylitol. Cazón et al. 2018 reported transparency levels of 13.67–36.25% for cellulose–glycerol–polyvinyl alcohol composite films, and 15–20% for low-density polyethylene films. Also, Lee, Son, & Hong (2008) obtained polypropylene films of 38.2% transparency and Park et al. 2020 reported transparency level of 26.2% and 30.4% for CNF/epoxy films. As can be seen, the transparency values of our CNC-based films are similar to those reported for some synthetic polymers.

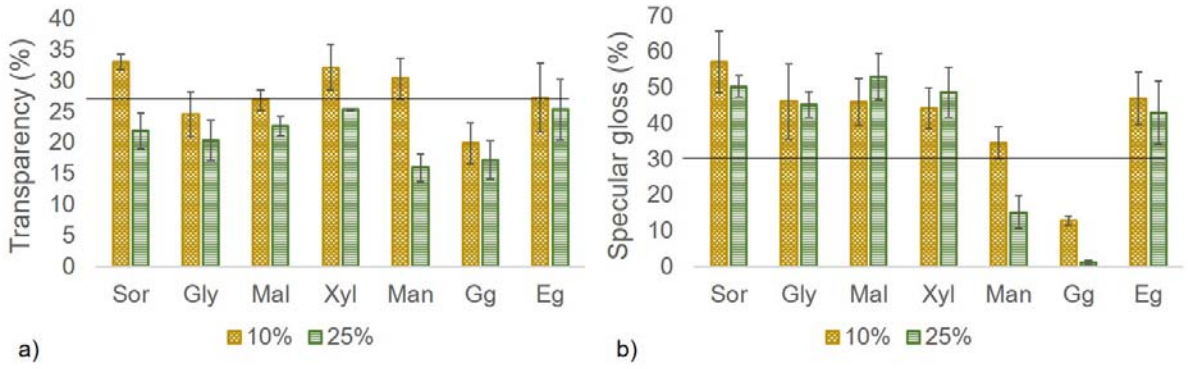

Fig. 1. Transparency [a), as calculated from eq. 2] and specular gloss [b)] of CNC-based films containing additives at a dose of 10 or 25% as compared to the additive-free control film (line).

Light absorption measurements were used to assess the ability of the films to protect from UV radiation. Figure S2 in supplementary material shows that absorption in the 200–400 nm range (UV region) was higher in the films containing an additive. The highest light absorption was found in those films that provided the lower specular gloss (Gg followed by Man). Then, Sor, Gly, Mal, Xyl and Eg showed similar light absorption

behavior. The plasticizers thus increased film transparency and UV protection, so they might be useful for food packaging purposes. Similar results were previously reported by Cazón et al. (2018), who found cellulose–glycerol films to have a UV protective effect. Glycerol also proved an effective UV protector in hydroxypropylmethyl cellulose films (Imran et al., 2012).

Mechanical properties

The industrial usefulness of CNC-based films is severely limited by their brittleness and difficult handling. Adding a plasticizer, however, decreases interactions between nanocellulose crystals, thereby making films more flexible and less brittleness, and preventing breakage during handling. Film plasticity is mainly governed by the mechanical properties like tensile strength (TS) and elongation (Ɛ) [42].

The effect of the additives was assessed by characterizing resulting films in terms of TS, Ɛ and Young's modulus (E) for comparison with a control film (Table S2 in supporting information). The high dispersion in the data may have arisen by internal tensions that occur during the drying process of film formation. Tardy et al. 2019 reported that capillary stresses take place during the casting process of CNC films, producing structural defects and deforming the substrate. Baez et al. 2014 investigated how the drying method of the CNF films affected tensile data scatter. The films containing no additive (control film) were brittle and poorly resistant compared to other types of films. They had a tensile strength of 15 MPa and a tensile index of 15 Nm g–1. Gao et al. 2017 reported a TS value of 38.5 MPa for alginate films with no additive, and Fillat et al. 2018 obtained tensile index values around 18 Nm g–1 for bacterial nanocellulose films. As can be seen from Figure 2a), most of the additives increased the tensile strength with respect to the control film. In fact, all films containing an additive were more easily handled; with the exception of those containing Gg which were also more difficult to peel off the cast owing to their high stickiness.

The influence of plasticizer amount was found to depend on the type of additive [Figure S3 a)], and most additives decreased TS when used above a given dose. This occurred because the plasticizer is placed between the polymer molecules, leading to greater intermolecular spacing of the cellulose chains. Talja et al. 2007 and Ili Balqis et al. 2017 also obtained a diminution in TS with the increase in plasticizer concentration in carraggenan films and potato starch-based films, respectively. Csiszár and Nagy 2017 studied how Sor and Gly and their concentrations affected the tensile strength of CNC films and they proved the optimal amount was 15% for both plasticizers, although sorbitol provided significantly higher TS than glycerol. Yang et al. 2016 studied the effect of Sor and Gly in protein films and also found that Sor formed stronger films than Gly, due to the

lower molecular weight of Gly. Mathew and Dufresne 2002 obtained better results with Sor than with Gly in maize starch films, but Mal was the most efficient at higher RH levels in terms of tensile index. Navarro-Tarazana et al. 2008 found Man increased TS of hydroxypropyl methylcellulose-beeswax film to a greater extent than Gly. In our CNC-based films xylitol and maltitol showed better tensile strength properties than sorbitol and glycerol at 15%, and in addition xylitol provided the highest TS value with only an amount of 10% [Figure S3 a)].

As can be seen from Figure 2b), all additives except Man and Eg improved elongation at break (Ɛ) as the amount was increased. These results are consistent with other works reported by Csiszár & Nagy, 2017; Ili Balqis et al., 2017 and Talja et al., 2007, who added sorbitol and glycerol to CNC, carrageenan and potato starch, respectively.

Ili Balqis et al. 2017, stated that glycerol and sorbitol made the films more stretchable and flexible, since they contributed to increasing the mobility of polymer chains. Xyl was the most efficient plasticizer as it reached to provide an elongation 3 times higher than the control film [Figure S3 b)].

Young's modulus (E) results decreased with increasing additive dose [Figure 2c)]. This behaviour was also reported by Talja et al. 2007 and Gao et al. 2017 in potato starch and alginate films, respectively.

At the highest additive dose, all films had a smaller E value than the control sample [Figure S3 c)]. However, Mal, Man and Eg at the lowest dose increased the moduli of the films relative to the control sample. In fact, the obtained E values were greater than others previously reported for CNC-based films. Thus, Csiszár et al. (2017) obtained E values below 6.5 and 3 GPa for CNC films containing sorbitol and glycerol, respectively, whereas our values covered the ranges 7.3–9.3 and 9.1–11.2 GPa, respectively.

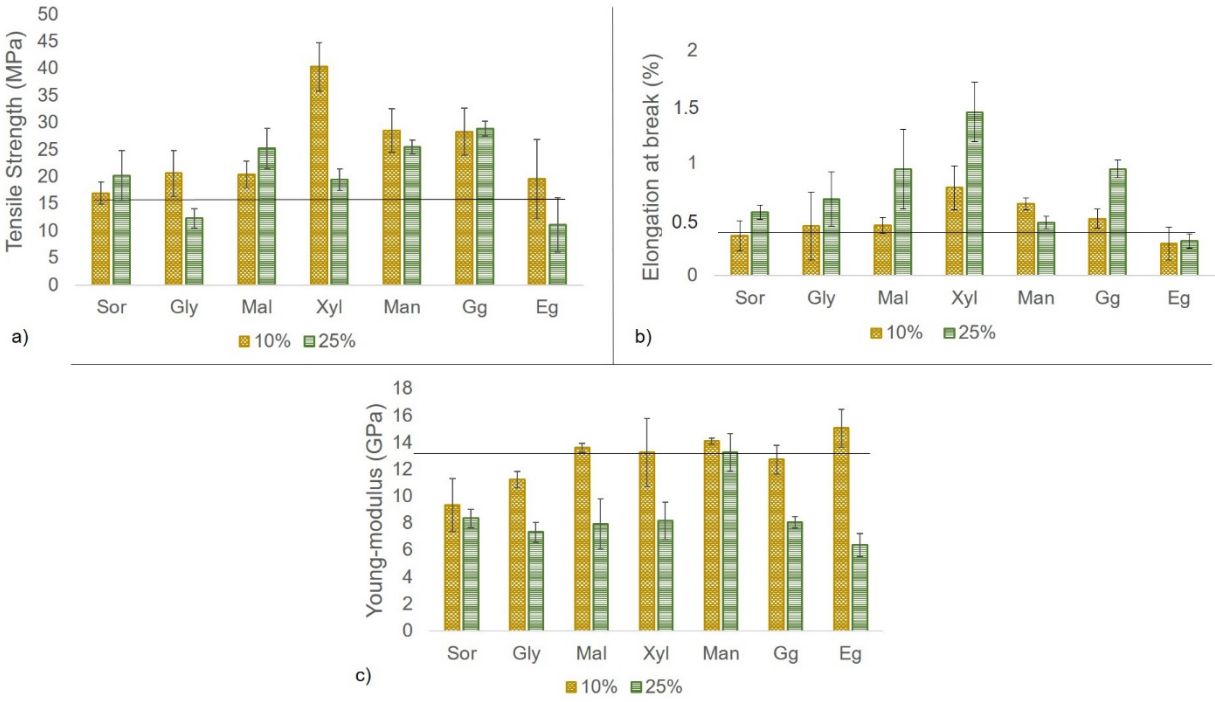

Fig. 2. Tensile strength [a)], Elongation at break [b)] and Young-modulus [c)] of the control film (line) and the films containing an additive (columns).

Thus, as the results show, the addition of a plasticizer in a CNC film improved the plasticity and handling of the film, preserving its tensile strength. Xylitol is shown as the most suitable additive for the production of CNC films in terms of mechanical properties.

Film structure and morphology

Theoretical porosity

The values of basis weight, thickness and apparent density of the films used to measure the theoretical porosity are shown in table S3 (supporting information). Changes in film morphology by effect of the additive were examined in terms of theoretical porosity. As can be observed from the porosity results of control= 25.38 ± 5.93% and plasticizers at 25% (Gly= 28.61 ± 4.17%, Xyl= 20.95 ± 2.10%, Eg= 20.89 ± 2.83%, Gg=19.05 ± 6.28%, Sor= 17.90 ± 1%, Man= 11.78 ± 2.10% and Mal= 7.11 ± 1.44%), all additives except Gly decreased porosity to a greater or smaller extent. Csiszár & Nagy (2017) also calculated theoretical porosity of CNC films, however they did not find a remarkable difference when glycerol or sorbitol were added as plasticizers.

Roughness

290 Film roughness was also studied because it can restrict the use of films for purposes such as electronic
291 circuit printing. The control film had a slightly less roughness (315 ± 89 ml/min, Figure 3) than for example
292 conventional printing papers but higher than bacterial nanocellulose films (24-30 ml/min, Fillat et al. 2018).
293 Also, all additives except Man and Gg decreased film roughness to values below 50 ml/min. Therefore, adding a
294 plasticizer generally increases film smoothness.

295 High roughness, and a dose-dependent increase in roughness was obtained when Gg and Man were
296 used. As can been observed in Figure S4 (supplementary material), the films containing Gg or Man exhibited a
297 less uniform and compact structure. This result along with morphological differences observed in the films, may
298 be indicative of a lower interaction within CNC, by virtue of the presence of such additives. For example, these
299 compounds provided the lowest film transparency and gloss, which could be due to a less cohesive structure,
300 promoting light scattering. The decreased CNC-plasticizer interaction is evident in the case of Gg. When high
301 doses were used (i.e. 20% and 25%), an embrittlement was observed, producing the film rupture, and making
302 impossible to measure the roughness. Also, the casting suspensions with Gg and Man showed higher viscosity,
303 with respect to the rest of the additives. The increase on viscosity was visually observed and was so evident that
304 even complicated the handling of the suspension. The increased viscosity produces a greater resistance to
305 spreading and may increase surface roughness, as observed previously [48].

306 Since the chemical formula of Man and Sor is the same, we could have expected similar behaviors for
307 these two compounds. However, there is an important difference in the hydroxyl group of the second carbon,
308 which has different configuration. Thus, these two compounds are epimers, and present different chemical
309 properties. The main differences are in their melting points, and that sorbitol is considered very hygroscopic,
310 while mannitol is considered non-hygroscopic [49,50]. Given that the cohesion of a CNC film is achieved upon -HO
311 interactions with water, the presence of a non-hygroscopic compound like Man, may have hindered the hydrogen
312 bond interactions, resulting in a less-cohesive structure.

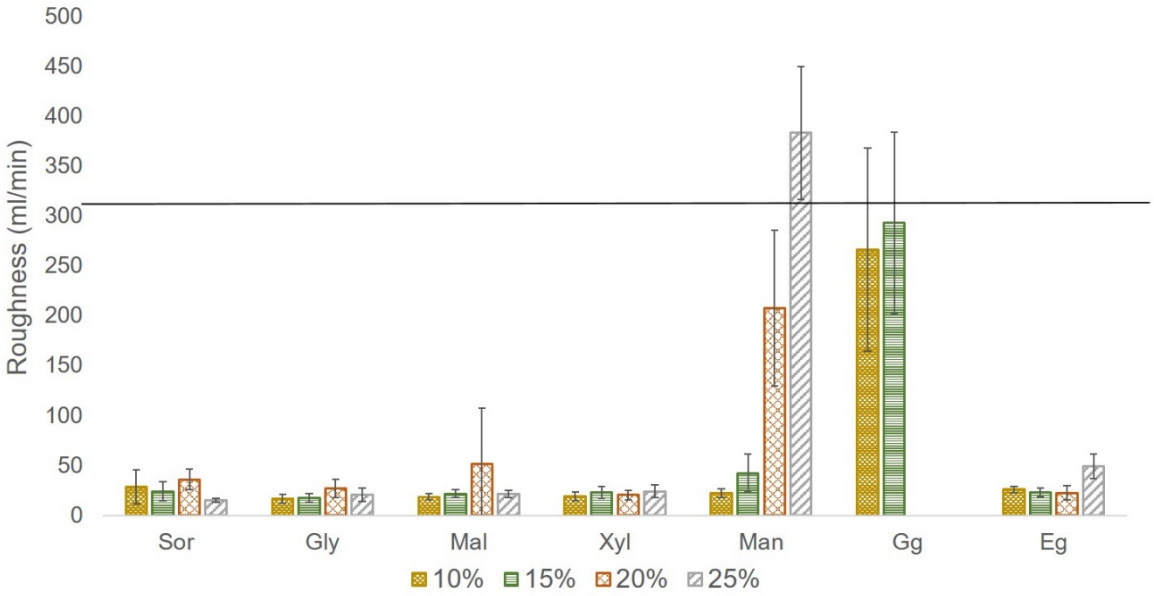

313

314 **Fig. 3.** Effect of the type of plasticizer and its dose on roughness (%) relative to the control film (line).

315 Film morphology by SEM

316 The effect of the additives on film morphology and structure was also examined from cross-sectional
317 scanning electron micrographs. The micrographs for the films containing no additive (Figure 4a and 4b)
318 exhibited a fairly ordered nanocrystal arrangement and a highly linear layered structure. Similar layered
319 structures were previously observed in other CNC films that retained the self-assembling ability of suspended
320 cellulose nanocrystals after evaporation [36,51].

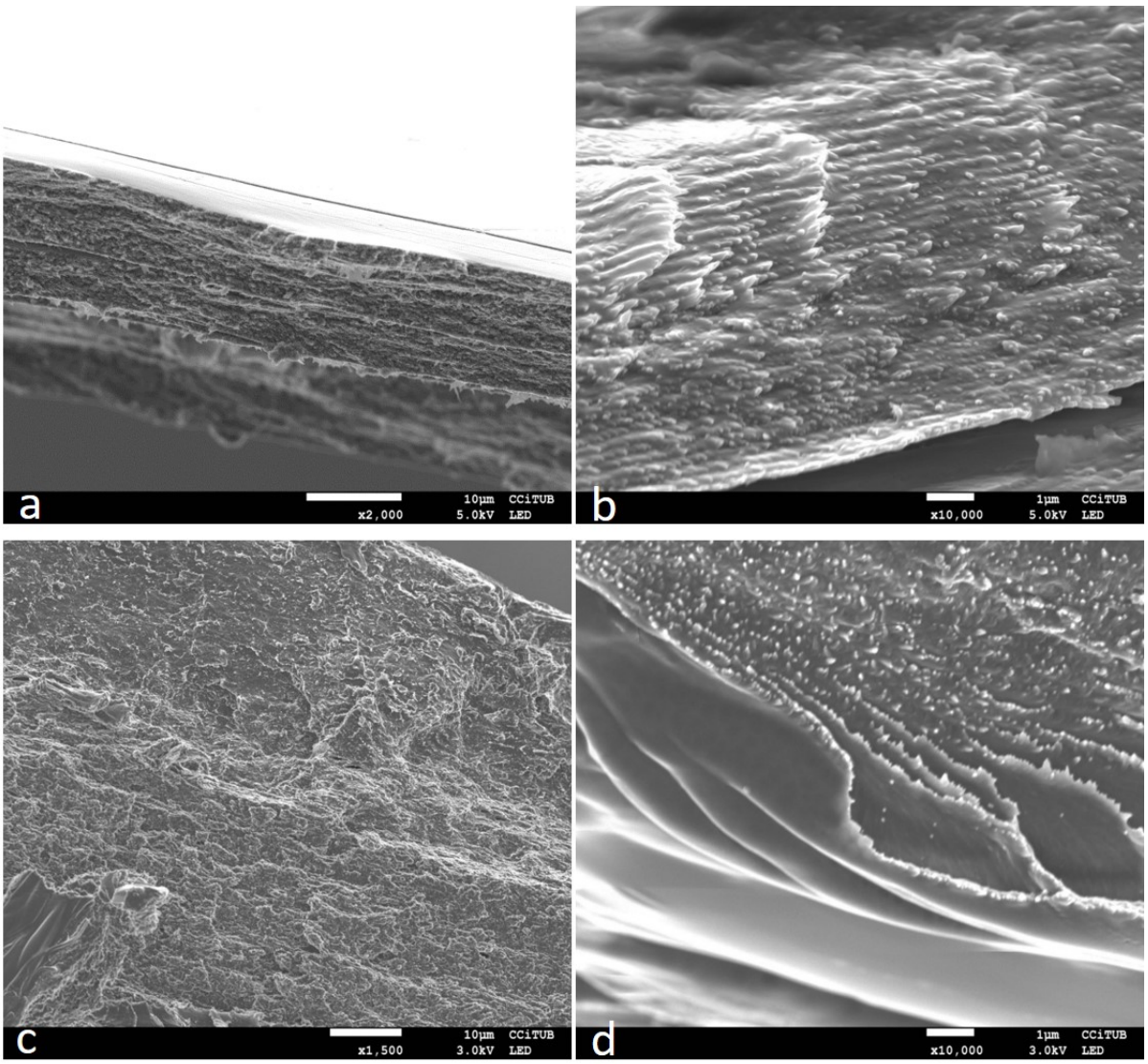

Fig. 4. Scanning electron micrographs of the control film (a and b) and the films containing 25% Sor (c and d).

The effect of the additives is illustrated with the film containing 25% Sor in Figure 4c and 4d (all others behaved similarly). As can be seen from the micrographs, there were no appreciable differences from the control film. However, the presence of a plasticizer led to smoother layers or surfaces, producing a more compact and uniform film. Bardet et al., 2015 investigated CNC–poly(ethyleneglycol) interactions and found the resulting films retained the self-assembling ability of CNC and had smoother surfaces. According to Tyagi, Hubbe, Lucia, & Pal (2018), a compact matrix can provide an effective barrier against gases and moisture.

Barrier properties

Many food packaging materials are petroleum-derived polymers. These are inexpensive, easy to handle and impermeable, but pose serious environmental problems. Hence the existing interest in improving the barrier properties of nanocellulose films.

Air permeance

Air permeance is one interesting barrier property to maintain the quality of packaged foods and increase shelf-life. The permeance of the additive-free film (2.03 ± 0.14 µm Pa^{-1} s^{-1}, Figure 5) was much lower than that of wood fibre paper but slightly higher than that of bacterial nanocellulose films (1.3 ± 0.1 µm Pa^{-1} s^{-1}, Fillat et al. 2018). All additives decreased air permeance to values from 0.95 ± 0.10 to 1.82 ± 0.12 µm Pa^{-1} s^{-1}, however the dose of plasticizer did not influence this property. Higher resistance to air penetration was expected as plasticizers decreased the theoretical porosity of the films. The lowest permeance was that of the film containing 10% Sor and the highest that of the Gg-containing films.

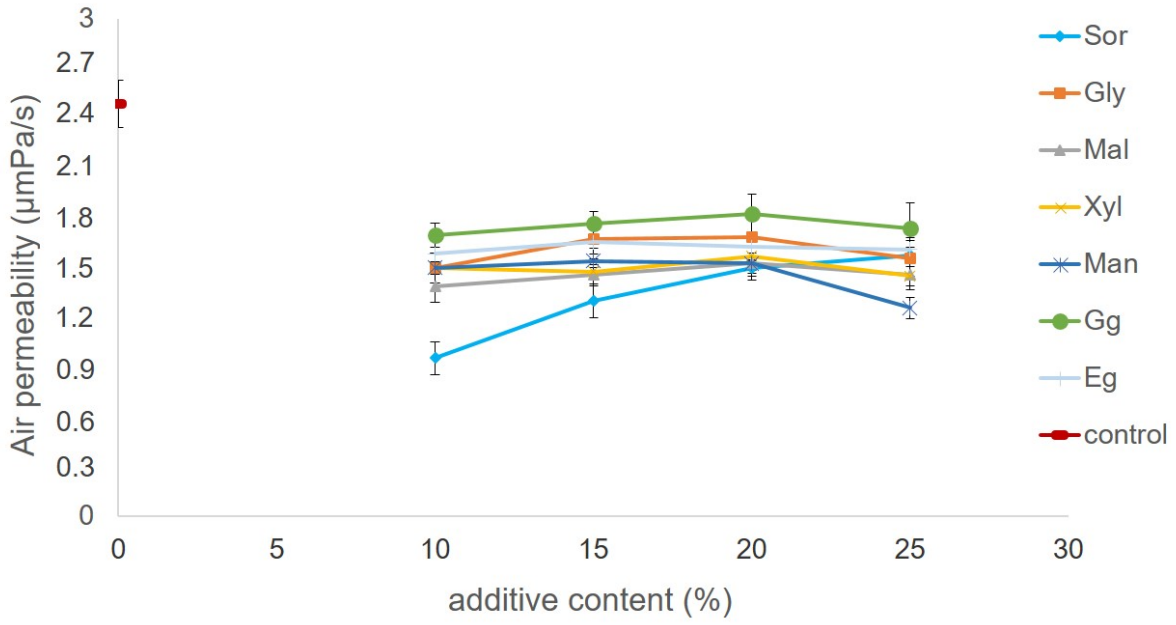

Fig. 5. Air permeance (µm Pa^{-1} s^{-1}) of the CNC-based films, at different doses of additive.

Oil resistance

Oil resistance is one of the most important properties of films with a view to their use as food packaging materials. We measured oil resistance in the films containing a 10% and 25% dose of each additive and in the control film for comparison (the methodology performed to carry out the essay is shown in supporting information, video "oil_resistance"). All CNC samples showed no penetration of oil through the films (relative

rate of oil penetration higher than 1800 s) therefore they were oil-proof. Neither the presence of an additive nor its dose altered the oil resistance of the films. Tyagi et al. 2018 also found an improvement of oil resistance when different packaging base papers were coated with CNC and sodium montmorillonite as a co-additive. In fact, oil resistance is strongly influenced by air permeability [52,53]. The lower the air permeability, the greater the oil resistance. And as it is shown in Figure 5, air permeance of CNC-based films was actually very low.

Water permeance

The high affinity of cellulose for water restricts its use in liquid containers. Figure 6 shows the time needed by each film to absorb a drop of water as measured with the water drop test (WDT). As can be seen, the control film exhibited a substantial water absorption resistance clearly exceeding that of paper fibre-based materials, which is typically less than 1 min. Moreover, the additives further decreased the water absorption capacity of the films, and this effect was more pronounced when the additive dose was increased.

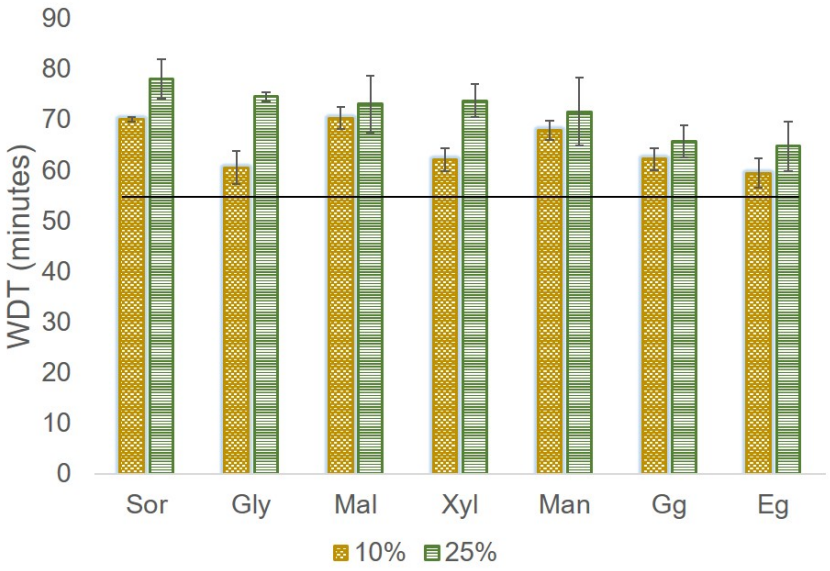

Fig. 6. WDT (min) of the CNC-control film (line) and CNC-based films additives (columns).

Hydrophobicity

The hydrophobicity of the films was evaluated by measuring the water contact angle. The WCA value for the control was 53.2° ± 0.10 (Figure 7) similar to those of cotton linter-based CNC films obtained by Beltramino et al. (2015). Moreover, all additives except for Gg caused a slight decrease in WCA. Xia et al. (2018) reported similar WCA values for cellulose nanofibers (CNF) films. They succeeded in increasing WCA up to 88° by a heating treatment, which caused an increase in surface roughness due to the fibril shrinkage by the dehydration of surface hydroxyl groups [55]. Our Gg-containing films had a WCA of 90.45° ± 5.68 which

indicated the increase in hydrophobicity. This behaviour might be related with the highest surface roughness (Figure 3), but especially with the decrease in surface free energy, which we will discuss later.

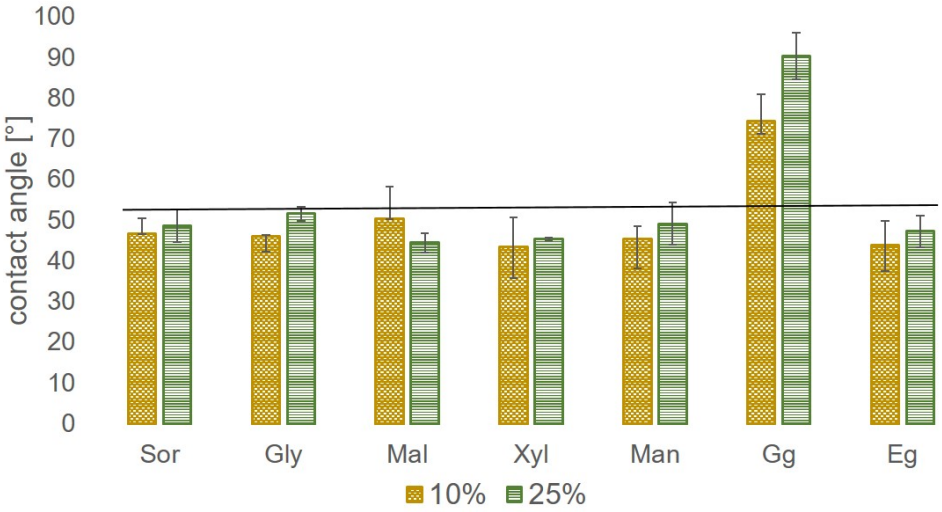

Fig. 7. Contact angle (°) of the control film (line- with a confidence interval of ± 0.10) and the films containing additives (columns).

Water vapor transmission rate (WVTR)

One of the most important drawbacks of polysaccharide-based films is their high water sensibility. This clearly limits their real life application, particularly in food packaging. Incorporation of biodegradable additives could improve barrier properties by making a network very hard for the molecules to pass through, due to an increased tortuosity. The WVTR was measured at 50% and 90% RH in those films that contained 25% of additives and all of them (except Gly and Eg) reached lower WVTR values at 50% RH than the un-plasticized film (172 g / m^2 * day, Fig. 8a). The lowest WVTR was recorded for films that contained Maltitol.

One of the most dominant factors in gas permeation is the rate of molecule diffusion in the film [56,57]. The transport phenomena into the film also depend on whether the gas interacts with cellulose or not [58]. However, the porosity is an aspect that should also be taken into account. It is known that gas permeability closely relates to the porosity or the ratio of void volume of the material. The volume of fluid (gas) will flow through the connected pores in the material or film. All films with plasticizers showed a lower theoretical porosity than the control, with the exception of the Gly which presented the highest water vapor permeation and also the highest theoretical porosity (Fig. 8a).

Higher values for WVTR were obtained under drastic humidity conditions (90%) (Fig. 8b). It has been reported that at 70% of relative humidity the hygroscopicity of these additives increases [59]. Mal was still the additive that presented the lowest WVTR value. In fact, only Mal and Gg were below the control. Zhang & Han, 2006 also obtained lower WVTR in pea starch films plasticized with Mal in comparison with those films plasticized with Gly and Sor. They stated that glucose in the Mal structure increased interactions between starch and Mal resulting in a more compact structure.

Although it was expected an increase in WVTR with the number of OH, the inverse effect was obtained (Figure 8b). The WVTR was higher with those plasticizers that had lower amount of OH groups. Zumbé et al., 2001 obtained that Xyl (5 OH) had higher hygroscopicity at 90ºC than Sor (6 OH), Man (6 OH) and Mal (9 OH). The highest WVTR was obtained with Gly (3 OH). Gly has also been reported to provide higher WVTR than other additives when it was applied in pea starch films [60], in pullulan-based blend films [61]. Sothornvit and Krochta 2001 and Lee et al. 2015 reported that Gly presents higher WVTR values because it is more hygroscopic. Ili Balqis et al. 2017 obtained that the WVTR decreased when sorbitol and glycerol were added to carrageenan films, but started to increase with increasing plasticizer concentration, except in the case of sorbitol that maintained the WVTR values even at the highest concentration. They attributed this behaviour to the higher hygroscopicity of glycerol, which increased the moisture content producing an increase in the effective diffusion coefficient.

In fact, Gly is a small molecule (3C) with three OH groups oriented in the same direction, which makes diffusion of water easier. Contrariwise, Sor is bigger (6C) and has its 6 OH groups oriented in different directions (mostly to one side), which is why it may be more difficult for water to diffuse [38]. Finally, a relationship between WVTR and molecular weight (Table S1) of plasticizers was also appreciated (as higher the molecular weight, lower the WVTR).

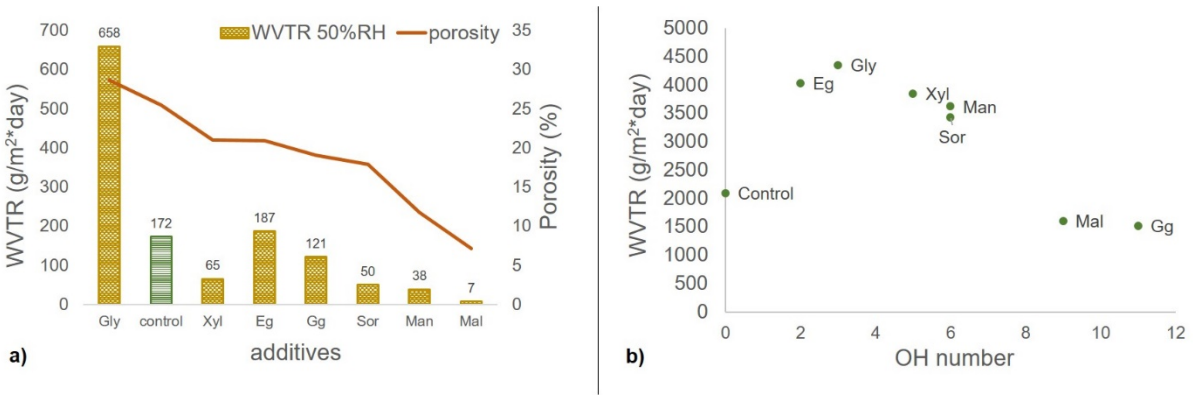

Fig. 8. Water vapor transmission rate (WVTR) a) at 50% RH and theoretical porosity, b) at 90% RH and the OH group content.

Oxygen permeability (OP)

The development of low oxygen transmission films is important in order to design barrier materials of great interest in the field of food packaging. At 20% RH, control film presented OP values of 1,806 $cm^3 \cdot \mu m/m^2 \cdot day \cdot atm$, being even higher (40,000 $cm^3 \cdot \mu m/m^2 \cdot day \cdot atm$) at 40% RH. Belbekhouche et al., 2011 obtained that CNC-based film were much more permeable to gases than microfibrillated cellulose (MFC) films. They explained that the lower packing of CNC particles increased mobility of gas molecules through the film, in comparison with the MFC structure which increased the tortuosity of the diffusion pathway.

OP was measured with those additives that provided the most interesting properties measured previously (CNC-Gly, CNC-Xyl, CNC-Sor and CNC-Mal at 25%). With the exception of Gly, additives provided films with better barrier properties compared to CNC control film (Figure 9). As in the case of WVTR, the higher oxygen permeability of the film with Gly can be related to its greater theoretical porosity. CNC-Gly film showed more theoretical porosity than the control, indicating that it had a more open structure that facilitated gas flow through the film.

Interestingly, CNC-Xyl, CNC-Sor and CNC-Mal films showed a totally resistance to oxygen from 20% RH until 60% RH. From then on, the OP started to increase, but always remained at values below the control at 40% RH. Recently, Gao et al. 2020 obtained oxygen permeability values for microfibrillar cellulose and chitosan films higher than those obtained with our films (566.73 $cm^3/m^2 \cdot day$ and 246.03 $cm^3/m^2 \cdot day$ when the amount of chitosan increased). And also Jung et al. 2020 reported values for a clean PLA film (without the addition of another compound) of 32.26 $cc \cdot mm/m^2 \cdot day \cdot atm$ at 0% RH. Wang et al., 2018, stated, as high grade of oxygen permeability, values below 40 $cm^3 \cdot \mu m/m^2 \cdot day \cdot atm$, and also published OP values at 90% RH for polypropylene (PP) of 100,000 $cm^3 \cdot \mu m/m^2 \cdot day \cdot atm$ and for polyethylene (PE) of 200,000 $cm^3 \cdot \mu m/m^2 \cdot day \cdot atm$; those values are greater than the values that were obtained from our additive-containing CNC films.

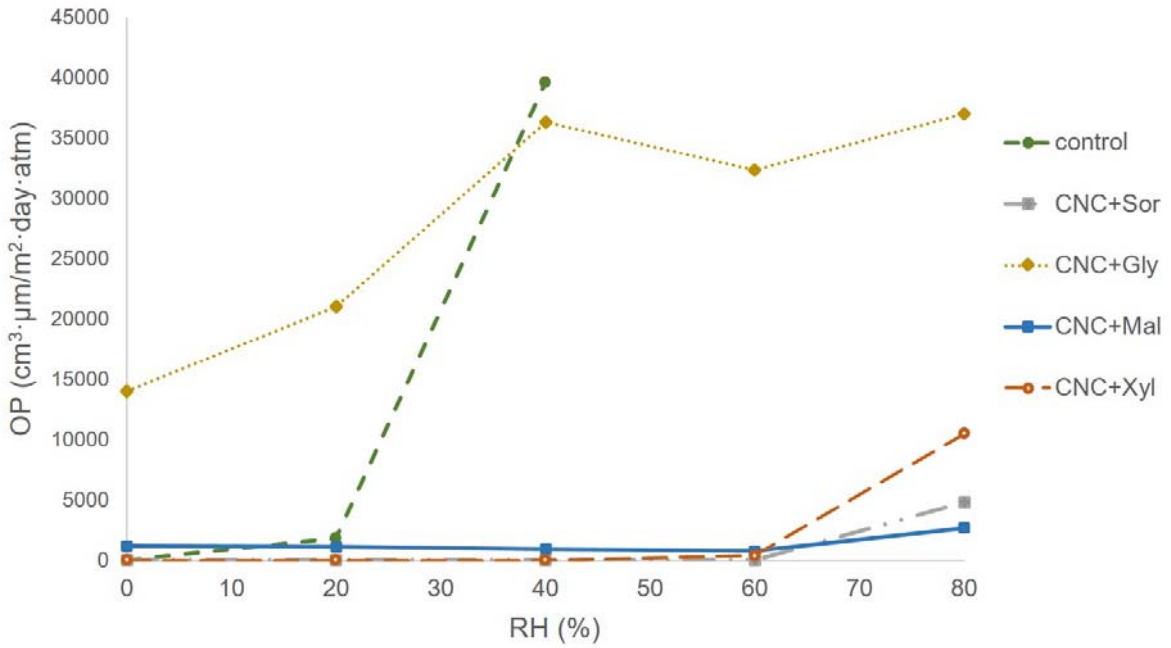

Fig. 9. Oxygen permeability (OP) of control and additive-containing films (Sor, Gly, Mal and Xyl).

It is well-known that high barriers towards oxygen and water vapor permeation are the most important limiting factors considered for modified atmosphere packaging (MAP) [57]. There was a correlation between the WVTR (50% RH) and OP (80% RH) results (figure 10). The different additives acted in coherence for both properties. This confirms the relationship between the number of OH in each additive and their behaviour for these properties. We can see that to higher number of OH, lower OP, as has been described in the previous section regarding WVTR. Gas barrier is usually obtained with the use of aluminium or a synthetic polymer. The polymer to choose depends on the type of barrier required: some can protect against water vapor but are permeable to oxygen, such as polyethylene (PE) [66]. Our films are proposed as a material with good barrier properties to both oxygen and water vapor, which makes it very interesting for possible packaging applications. Oxygen transmission between 40-400 cm3·µm/m2·day·atm are required for a high oxygen barrier film [64]. Considering the low OP values obtained, our films could be suitable as packaging material for foods such as fresh meat, peanuts and instant coffee since the required OP values are below 70 cm^3/m^2·day, 50 cm^3/m^2·day and 1 cm^3/m^2·day, respectively (Wang et al. 2018, Gao et al. 2020). Furthermore, the Mal film would also meet the requirements in terms of WVTR.

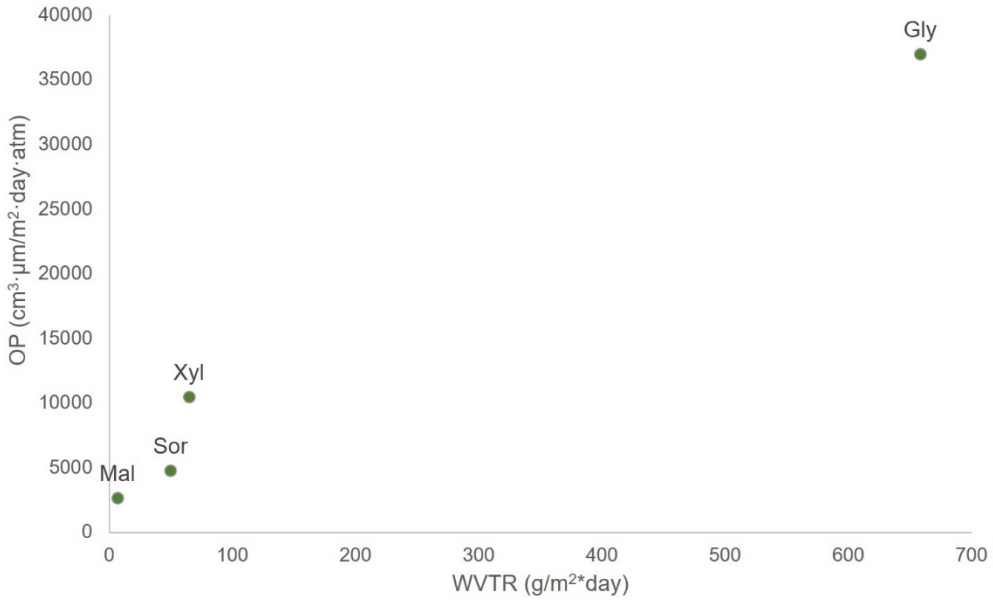

Fig. 10. Oxygen permeability (OP) at 80% RH and water vapor transmission rate (WVTR) at 50% RH of control and additive-containing films (Sor, Gly, Mal and Xyl).

Surface free energy (SFE)

The surface free energy represents a very interesting information regarding industrial implementation of the films, i.e. in predicting which liquids or adhesives may successfully interact with our films. As shown in Figure 11, values of SFE go from 34.32 mJ/m^2 to 48.47 mJ/m^2. Results obtained of SFE are in accordance with previous values described for CNC-based films. Sun et al. 2018 obtained higher values (from 42.55 mJ/m^2 to 53.87 mJ/m^2) for CNC-CNF films. They stated that SFE increased with the content of CNF. This may be the reason of the lower value obtained in our films (that did not contain CNF). Similar than our results, Nagy et al. 2018 did not observe significant differences in the SFE when glycerol o sorbitol were added to CNC films. However, they obtained higher SFE values (around 76 mJ/m^2).

The CNC films containing additives show different energy states depending on the additive. Thus, their interaction with other compounds will differ, and a specific behaviour was identified for each additive. Sor, Gly and Xyl films showed an increased polar component, indicating their polar nature. The polar and dispersive components of the films containing Mal, Eg and Man were quite balanced. Finally, the film containing Gg was mainly dispersive, presenting also the lowest polar component.

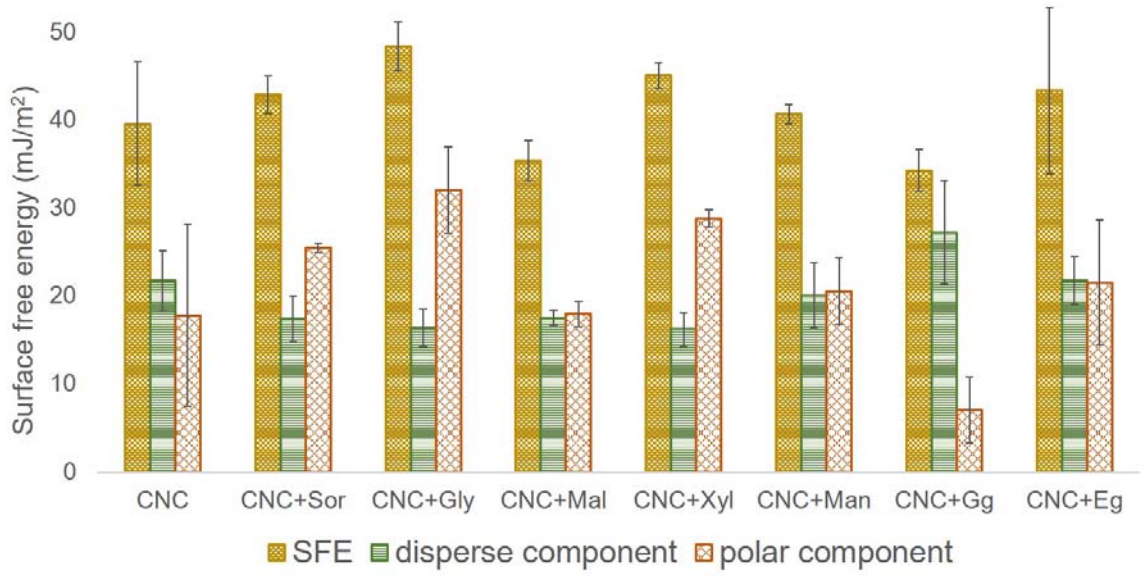

Fig. 11. Surface free energy (SFE) of the control film (CNC) and additive-containing films.

A relationship between the polar component and the number of OH groups in the chemical structure of the additive was observed (Figure 12). Thus, the higher the number of OH, the lesser the polar component. If we look at the nature of the additive having an increased number of OH, the Gg, we can observe (Figure 12) that it is more dispersive. This might be related to the contact angle results, where the largest contact angle was observed in the film containing Gg (90.45°); this could be attributed to the polarity of water (the liquid used in the determination of the contact angle). Thus, since Gg is a more dispersive compound, it results in a greater contact angle. The lack of interaction between water and Gg, may be associated to the large number of OH groups in the latter, resulting in an extended interaction (through H-bonding) with CNC and, therefore, decreasing the number of free -OH that may interact with water. Moreover, a correlation with the WVTR, when films were submitted at extreme humidity conditions can be appreciated (Figure 8b). The additive with the lowest polarity (the most dispersive), the Gg, showed the lowest values of WVTR. On the other hand, Gly, one of the most polar additives, showed the highest value for WVTR.

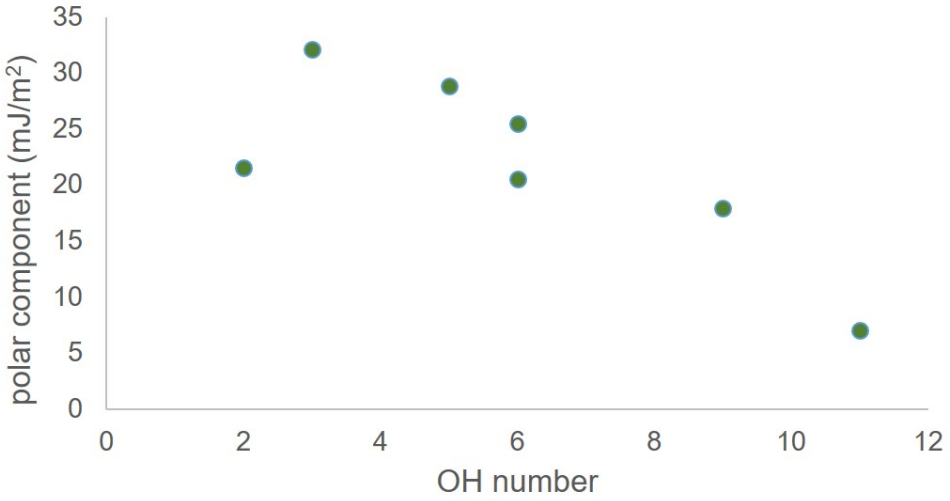

Fig. 12. Polar component and OH number of the additive-containing films.

Chemical structure of the films by FTIR

Figure 13 shows the Fourier transform infrared (FTIR) spectra for the control film and those containing an additive, which were used to detect specific, major chemical groups. Bands in the wavenumber region 3700–3000 cm^{-1} are typically assigned to stretching vibrations in hydroxyl groups [17], which are influenced by hydrogen bonds. Gao et al. 2017 previously found the strength of the band at 3258 cm^{-1} to peak with glycerol by effect of its high content in hydroxyl groups. Cazón et al. 2018 observed a similar behaviour in cellulose–glycerol–PVA films, and so did Rouhi et al. 2017 in PVA–glycerol films. As also obtained by these authors, the fact that our spectra exhibited no absorption band for free OH groups at 3600 cm^{-1} suggests that hydroxyl groups largely formed inter- and intramolecular hydrogen bonds. The bands at 2906 and 2890 cm^{-1}, can be assigned to aliphatic C–H bond stretching in alkyl groups, and the absorbance peak at 1640 cm^{-1} was assigned to H–O–H bending vibrations in adsorbed water. A peak at ca. 1050 cm^{-1} typical of cellulose and due to stretching vibrations of C–O–C bonds in pyranose rings of primary and secondary alcohols in cellulose was also observed. The peak at ca. 895 cm^{-1} was due to glycoside bonds in cellulose, and those in the region 800–650 cm^{-1} to O–H bond vibrations [69]. These results, which are very similar to those previously reported by [17], suggest that the additives caused no change in the chemical composition of CNC.

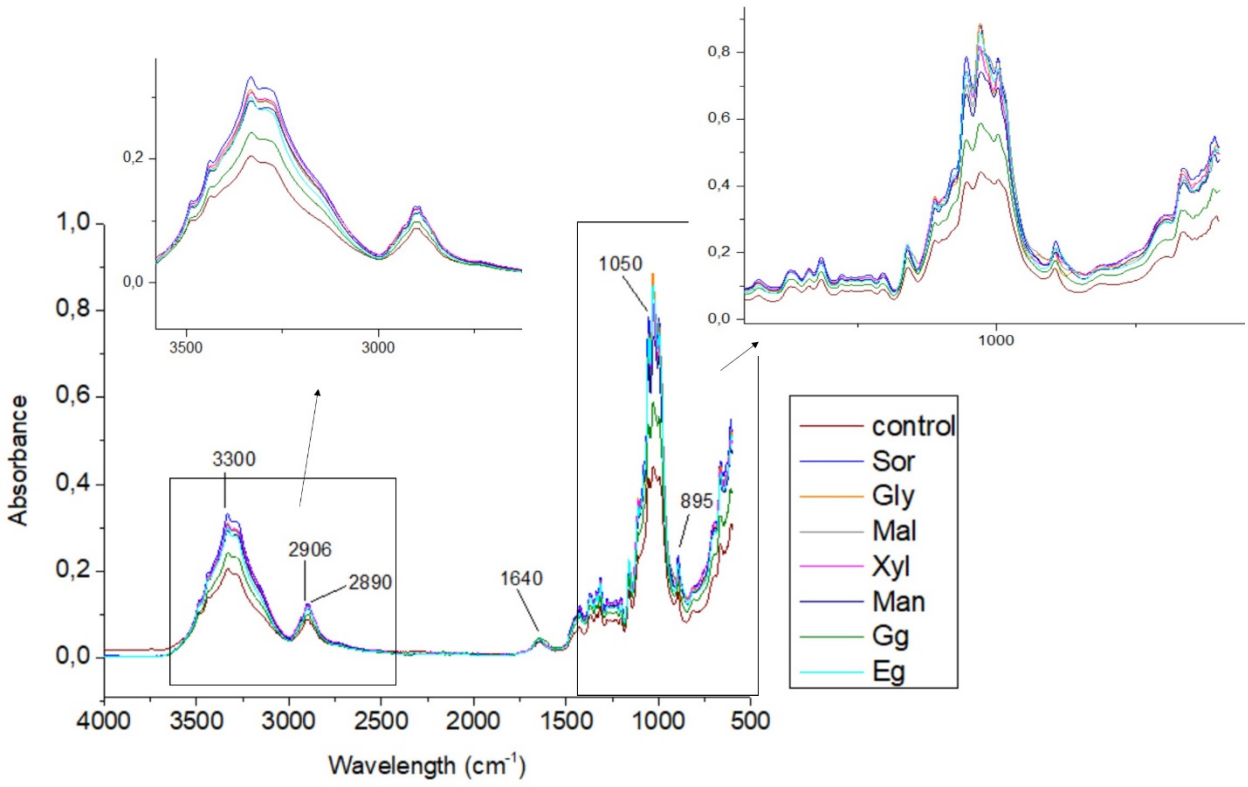

Fig. 13. FTIR spectra for the control and additive-containing films.

In addition to the analysis of films containing CNC and additives, the FTIR measurements of the pure additives were also performed (Figure S5), to reach a better understanding of their chemical structure and interaction with CNC. In this regard, we have identified a band in the region around 2900 cm^{-1} which can be directly linked to their chemical structure and used to observe differences between additives. The band becomes double-peaked when hydrocarbon chains are present in the structure of the additive. This is the case of Eg and Gly additives, which present a well-defined double peak, being also the ones with less -OH groups in their structure. The rest of the additives had higher number of –OH; thus, their hydrocarbon chains may had been masked by the presence of –OH groups, resulting in a difficult observation of the double peak (or even not observed at all, as occurs with Gg -with only one peak- since it has not hydrocarbon chains in its structure). The peak at 1600 cm^{-1} observed in Gg additive may be attributed to the carbonyl (C=O) double bond in the carboxyl group. The band corresponding to the C=O double-bond usually appears at other wavelengths, but may have been shifted due to H-bond interactions.

On the other hand, the FTIR patterns of pure additives and that of the CNC+additive mixtures were analysed individually for each additive. The height of the broad band appearing at the wavenumber region of 3400 cm^{-1} provides information about the interaction between the additive and CNC (Figure S6). If the bands are considered separately, several characteristic peaks corresponding to the pure additive start to appear in the

mixture pattern. For instance, in pure Gly [Fig. S6 a)] there is a characteristic double-peak around 2900 cm^{-1}, which can be slightly identified in the mixture pattern. Similar observation was found at 800 cm^{-1}, in both Gly and Mal spectra [Fig. S6 a) and Fig. S6 b), respectively]. In general, the shape of the spectra of the CNC+additive mixture is strongly linked to that of the pure additive and pure CNC. Characteristic peaks of the pure additive can be slightly identified in the mixed spectra, but not in pure CNC. These observations are restricted to some of the additives and mixtures considered. In the spectra corresponding to additive+CNC mixtures, it is important to take into account that the mixtures only contain 25% additive, meaning that in many cases, CNC may be masking the peaks corresponding to the pure additive.

Crystallinity of the films by XRD

Figure 14 shows the diffraction patterns for the control and modified films. The main diffraction angles at the 2θ values 14.88° (1–10), 16.58° (110) and 22.61° (200) correspond to primary diffraction in the (1–10), (110) and (200) planes of polymorph cellulose I [70].

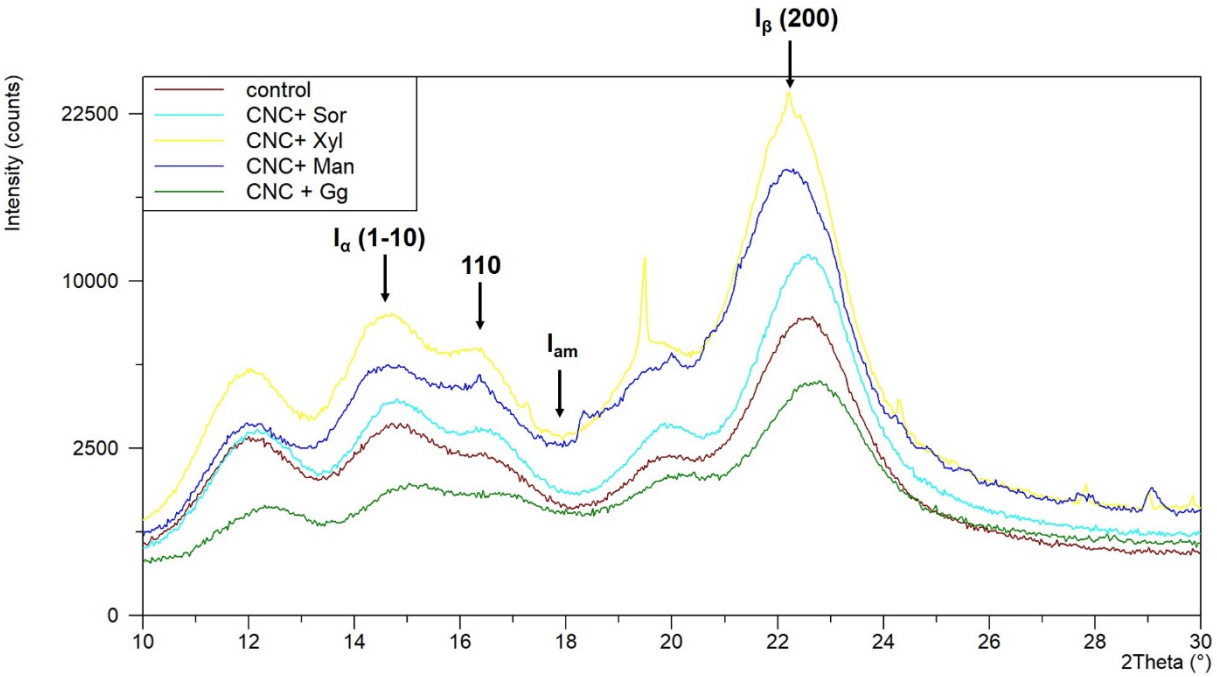

Fig. 14. XRD patterns for the control film and others containing Sor, Xyl, Man or Gg at a 25% dose.

The crystallinity index (CI) of the films was calculated from eq. 5 (Segal et al. 1959). The results show (Table S4 in supporting information) that crystallinity was higher in the films containing 25% Sor (CI = 88.84 %) or 25% Xyl (CI = 88.85 %) than in the control film (CI = 88.75 %). In contrast, crystallinity in the films containing 25% Man or 25% Gg was slightly lower than in the control film (85.66 and 82.1%, respectively). The

lower CI of Man and Gg may be explained by its lower interaction with CNC giving rise to a less cohesive structure, as previously stated with roughness results. Similar films were previously found to have CI values from 54 to 88% [71]. The CI values from this study fell near the upper end of the typical range and the presence of additives had no adverse effect on crystallinity.

The CI values for control film and that containing 25% Sor are consistent with those of other authors, which ranged from 87 to 94%, depending on the particular raw material used to obtain the cellulose nanocrystals [5]. Films containing CNC as an additive rather than the main component have much lower CI values (20–35%); also, such values increase with increasing proportion of CNC [69]. Consequently, CNC increases film crystallinity when used as an additive and results in a high crystallinity (up to 87.37%) when used as the main film component.

Biodegradability

Although the improved workability, flexibility and barrier properties of the CNC films using additives, its biodegradability preservation is essential in order to make them suitable to be used in different final applications. It has been reported that the addition of nanocellulose in several composites or films with polyvinyl alcohol [72], starch [73], natural and nitrile rubber [74,75] and PBAT [76] increases its biodegradability. The additives used are natural and therefore they are supposed to be biodegradable. However, to our knowledge, there are no previous studies that analyse and compare the biodegradability of the plasticizers used combined with nanocellulose films. Thus, the biodegradability of CNC films with additives was evaluated in this work for the first time. This study was carried out using the highest percentage of additive (25%) since we can assume that, if a greater quantity is biodegraded, smaller quantities imitate this behaviour.

Interestingly, after 90 days in compost, higher levels of degradation were found for the films which contained additives (Figure 15). No relationship was found in this case between biodegradability and the OH number or molecular weight of the plasticizer. The film that was more easily biodegraded was the one that contained Xyl, followed by Gg, Sor, Gly, Mal and Man. Recently, Gatidou et al. 2020[77] assessed the biodegradability of twenty food additives. Maltitol and xylitol were selected as natural sweeteners and they exceeded 60% of biodegradation by day 10 for xylitol and day 12.5 for maltitol. Therefore, although both sweeteners were readily biodegradable compounds, xylitol was also easily biodegraded. The evolution of biodegradability tested showed that the control film gives rise to a lower amount of accumulated CO_2, which suggested that the microorganisms have generated less CO_2 during their metabolism. Therefore, the films

563 containing the additives were more easily biodegraded. Although these films were more resistant to the
564 penetration of water, as observed with the WDT results, the presence of these additives made them more
565 accessible for the penetration of the enzymes produced by the microorganisms. In fact, it is well described that
566 the accessibility of enzymes to the cellulose chains is not related by its capacity to retain water [78]. The
567 biodegradability results obtained here are considered very important for the environmental justification of the
568 replacement of plastic materials, which are not biodegradable and entail a big problem both environmentally and
569 economically.

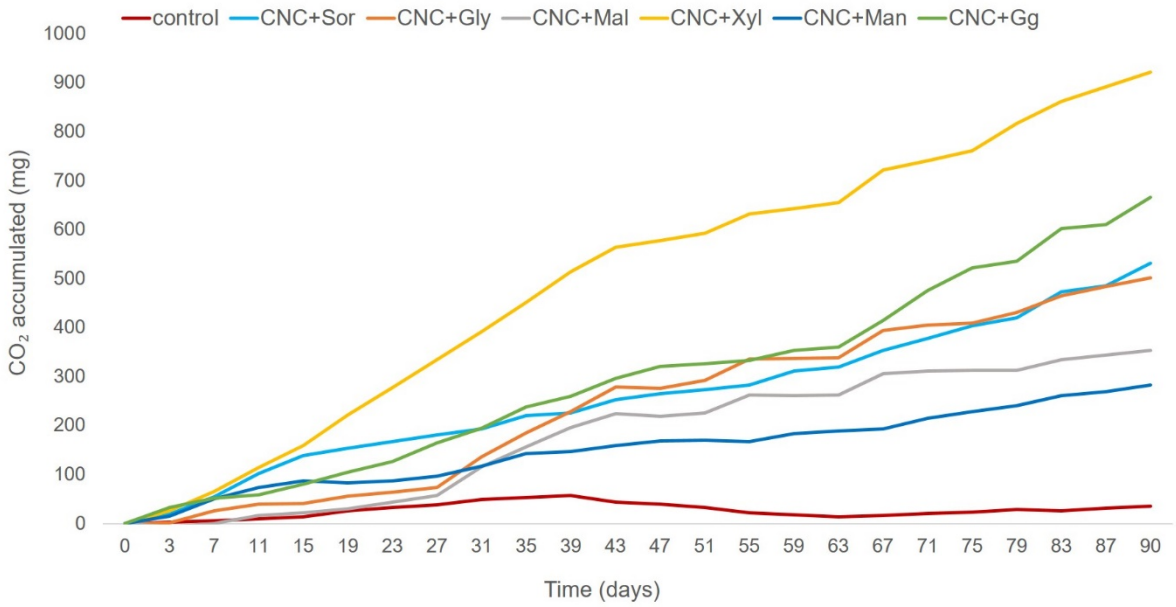

570

571 **Fig. 15.** Biodegradability, measured in accumulated CO_2 over time, of the films with the different additives
572 added in 25%, as well as the control.

573 **CONCLUSIONS**

574 CNC-based films obtained by adding a plasticizer (sorbitol, glycerol, maltitol, xylitol, mannitol, gellan
575 gum or ethylene glycol) at different concentration were characterized for optical, mechanical and barrier
576 properties, in addition for their biodegradability, for the first time. Based on the results, the additive dose used
577 influenced film transparency, which decreased with increasing dose. Thus, the films containing 10% Sor, Xyl or
578 Man were more transparent than the additive-free film. All additives, but particularly Gg, seemingly had a
579 protective effect against UV light; also, all increased tensile strength and elongation (except Eg and Man in
580 elongation), and decreased air and water permeance, to a greater or lesser extent. CNC films with Mal, Sor and
581 Xyl had better oxygen barrier than the control, showing a total oxygen resistance at RH below 60%. The Mal and

582 the Gg showed values of WVTR below the control, under both, moderate (50%) and drastic (90%) humidity. A
583 correlation has been observed between the number of OH contained in the different additives and their behaviour
584 against water vapor and oxygen. To higher OH number, lower WVTR and lower OP. For moderate humidities,
585 all additives except Gly and Eg have values below the control. These results are very interesting if we think
586 about the applicability of these films in the food packaging industry.

587 The film with a Sor dose of only 10% was the most transparent and least porous, and hence the most
588 resistant to air penetration and water absorption. On the other hand, the films containing Gg were those
589 exhibiting the greatest UV protection and hydrophobicity, whereas those containing Xyl were the most
590 mechanically effective and biodegradable. Finally, those containing Mal provided the best barrier properties to
591 oxygen and water vapor transmission. The analysis of the surface free energy of the films revealed different
592 behavior depending on the additive, providing valuable information regarding the interaction of the films with
593 other compounds i.e. liquids or adhesives. As was stated, the dose and type of additive provide a different effect
594 on the final properties of the film, which allows the most suitable additive to be chosen for the property required
595 in the film. It should be emphasized that all the additives increased the biodegradability of CNC-based films
596 when subjected to a biodegradability test under controlled composting conditions, for a period of 90 days. These
597 biodegradability results highlight the importance of using our films in the food industry, since they would
598 contribute to the reduction of environmental pollution caused by the materials traditionally used in food
599 packaging. Our films are presented as potential material in the organic food market, which is becoming more and
600 more important on a global scale.

601 **SUPPORTING INFORMATION**

602 Orthogonal and oblique projection; absorbance curves; mechanical properties with different percentages of
603 additives; optical micrographs; FTIR spectra of the different additives, FTIR spectra of CNC-based films
604 containing different additives; Chemical structure, OH number and molecular weight of additives; values of
605 mechanical properties; basis weight, thickness and apparent density; crystallinity index values.

606 **ACKNOWLEDGEMENTS**

607 The authors are grateful to the FILMBIOCEL (No. CTQ2016-77936-R) (funding also from the "Fondo
608 Europeo de Desarrollo Regional FEDER"), and MICROBIOCEL (No. CTQ2017-84966-C2-1-R), within the
609 framework of the Spanish's MINECO. The authors would also like to thank the consolidated research group

AGAUR 2017 SGR 30 with Universitat de Barcelona (UB) and to the Serra Húnter Fellowship awarded to O. Cusola.

REFERENCES

(1) Grishkewich, N.; Mohammed, N.; Tang, J.; Tam, K. C. Recent Advances in the Application of Cellulose Nanocrystals. *Curr. Opin. Colloid Interface Sci.* **2017**, *29*, 32–45. https://doi.org/10.1016/j.cocis.2017.01.005.

(2) Rubilar, J. F.; Candia, D.; Cobos, A.; Díaz, O.; Pedreschi, F. Effect of Nanoclay and Ethyl-Nα-Dodecanoyl-l-Arginate Hydrochloride (LAE) on Physico-Mechanical Properties of Chitosan Films. *LWT - Food Sci. Technol.* **2016**, *72*, 206–214. https://doi.org/10.1016/j.lwt.2016.04.057.

(3) Rhim, J.-W.; Hong, S.-I.; Park, H.-M.; Ng, P. Preparation and Characterization of Chitosan-Based Nanocomposite Films with Antimicrobial Activity. *J. Agric. Food Chem.* **2006**, *54*, 5814–5822. https://doi.org/10.1021/jf060658h.

(4) Herrera, M. A.; Mathew, A. P.; Oksman, K. Barrier and Mechanical Properties of Plasticized and Cross-Linked Nanocellulose Coatings for Paper Packaging Applications. *Cellulose* **2017**, *24* (9), 3969–3980. https://doi.org/10.1007/s10570-017-1405-8.

(5) Csiszár, E.; Nagy, S. A Comparative Study on Cellulose Nanocrystals Extracted from Bleached Cotton and Flax and Used for Casting Films with Glycerol and Sorbitol Plasticisers. *Carbohydr. Polym.* **2017**, *174*, 740–749. https://doi.org/10.1016/j.carbpol.2017.06.103.

(6) Beltramino, F.; Blanca Roncero, M.; Vidal, T.; Valls, C. A Novel Enzymatic Approach to Nanocrystalline Cellulose Preparation. *Carbohydr. Polym.* **2018**, *189* (February), 39–47. https://doi.org/10.1016/j.carbpol.2018.02.015.

(7) Tang, J.; Sisler, J.; Grishkewich, N.; Tam, K. C. Functionalization of Cellulose Nanocrystals for Advanced Applications. *J. Colloid Interface Sci.* **2017**, *494*, 397–409. https://doi.org/10.1016/j.jcis.2017.01.077.

(8) Dufresne, A. *Nanocellulose From Nature to High Performance Tailored Materials*; 2012.

(9) Beltramino, F.; Roncero, M. B.; Vidal, T.; Torres, A. L.; Valls, C. Increasing Yield of Nanocrystalline Cellulose Preparation Process by a Cellulase Pretreatment. *Bioresour. Technol.* **2015**, *192*, 574–581. https://doi.org/10.1016/j.biortech.2015.06.007.

(10) Csiszar, E.; Kalic, P.; Kobol, A.; Ferreira, E. D. P. The Effect of Low Frequency Ultrasound on the Production and Properties of Nanocrystalline Cellulose Suspensions and Films. *Ultrason. Sonochem.*

2016, *31*, 473–480. https://doi.org/10.1016/j.ultsonch.2016.01.028.

(11) Lam, E.; Male, K. B.; Chong, J. H.; Leung, A. C. W.; Luong, J. H. T. Applications of Functionalized and Nanoparticle-Modified Nanocrystalline Cellulose. *Trends Biotechnol.* **2012**, *30* (5), 283–290. https://doi.org/10.1016/j.tibtech.2012.02.001.

(12) Julkapli, N. M.; Bagheri, S. Progress on Nanocrystalline Cellulose Biocomposites. *React. Funct. Polym.* **2017**, *112*, 9–21. https://doi.org/10.1016/j.reactfunctpolym.2016.12.013.

(13) Beck, S.; Bouchard, J.; Berry, R. Controlling the Reflection Wavelength of Iridescent Solid Films of Nanocrystalline Cellulose. *Biomacromolecules* **2011**, *12*, 167–172. https://doi.org/https://doi.org/10.1021/bm1010905.

(14) Habibi, Y.; Lucia, L. A.; Rojas, O. J. Cellulose Nanocrystals : Chemistry , Self-Assembly , and Applications. *Chem. Rev.* **2010**, *d* (6), 3479–3500. https://doi.org/10.1021/cr900339w.

(15) Aulin, C.; Gällstedt, M.; Lindström, T. Oxygen and Oil Barrier Properties of Microfibrillated Cellulose Films and Coatings. *Cellulose* **2010**, *17* (3), 559–574. https://doi.org/10.1007/s10570-009-9393-y.

(16) Montero, B.; Rico, M.; Rodríguez-Llamazares, S.; Barral, L.; Bouza, R. Effect of Nanocellulose as a Filler on Biodegradable Thermoplastic Starch Films from Tuber, Cereal and Legume. *Carbohydr. Polym.* **2017**, *157*, 1094–1104. https://doi.org/10.1016/j.carbpol.2016.10.073.

(17) Cazón, P.; Vázquez, M.; Velazquez, G. Cellulose-Glycerol-Polyvinyl Alcohol Composite Films for Food Packaging: Evaluation of Water Adsorption, Mechanical Properties, Light-Barrier Properties and Transparency. *Carbohydr. Polym.* **2018**, *195* (January), 432–443. https://doi.org/10.1016/j.carbpol.2018.04.120.

(18) Jannatyha, N.; Shojaee-Aliabadi, S.; Moslehishad, M.; Moradi, E. Comparing Mechanical, Barrier and Antimicrobial Properties of Nanocellulose/CMC and Nanochitosan/CMC Composite Films. *Int. J. Biol. Macromol.* **2020**, *164*, 2323–2328. https://doi.org/10.1016/j.ijbiomac.2020.07.249.

(19) Muscat, D.; Adhikari, B.; Adhikari, R.; Chaudhary, D. S. Comparative Study of Film Forming Behaviour of Low and High Amylose Starches Using Glycerol and Xylitol as Plasticizers. *J. Food Eng.* **2012**, *109* (2), 189–201. https://doi.org/10.1016/j.jfoodeng.2011.10.019.

(20) Vieira, M. G. A.; Da Silva, M. A.; Dos Santos, L. O.; Beppu, M. M. Natural-Based Plasticizers and Biopolymer Films: A Review. *Eur. Polym. J.* **2011**, *47* (3), 254–263. https://doi.org/10.1016/j.eurpolymj.2010.12.011.

(21) Rouhi, M.; Razavi, S. H.; Mousavi, S. M. Optimization of Crosslinked Poly(Vinyl Alcohol) Nanocomposite Films for Mechanical Properties. *Mater. Sci. Eng. C* **2017**, *71*, 1052–1063.

https://doi.org/10.1016/j.msec.2016.11.135.

(22) Jost, V.; Langowski, H. C. Effect of Different Plasticisers on the Mechanical and Barrier Properties of Extruded Cast PHBV Films. *Eur. Polym. J.* **2015**, *68*, 302–312. https://doi.org/10.1016/j.eurpolymj.2015.04.012.

(23) Sirviö, J. A.; Visanko, M.; Ukkola, J.; Liimatainen, H. Effect of Plasticizers on the Mechanical and Thermomechanical Properties of Cellulose-Based Biocomposite Films. *Ind. Crops Prod.* **2018**, *122* (March), 513–521. https://doi.org/10.1016/j.indcrop.2018.06.039.

(24) Souza, A. C.; Benze, R.; Ferrão, E. S.; Ditchfield, C.; Coelho, A. C. V.; Tadini, C. C. Cassava Starch Biodegradable Films: Influence of Glycerol and Clay Nanoparticles Content on Tensile and Barrier Properties and Glass Transition Temperature. *LWT - Food Sci. Technol.* **2012**, *46* (1), 110–117. https://doi.org/10.1016/j.lwt.2011.10.018.

(25) Chen, P.; Xie, F.; Tang, F.; McNally, T. Influence of Plasticiser Type and Nanoclay on the Properties of Chitosan-Based Materials. *Eur. Polym. J.* **2021**, *144* (October 2020), 110225. https://doi.org/10.1016/j.eurpolymj.2020.110225.

(26) Navarro-Tarazana, M.; Sothornvit, R.; Pérez-Gago, M. Effect of Plasticizer Type and Amount on Hydroxypropyl Methylcellulose - Beeswax Edible Film Properties and Postharvest Quality of Coated Plums (Cv. Angeleno). *J. Agric. Food Chem.* **2008**, 9502–9509. https://doi.org/https://doi.org/10.1021/jf801708k.

(27) Mathew, A. P.; Dufresne, A. Plasticized Waxy Maize Starch: Effect of Polyols and Relative Humidity on Material Properties. *Biomacromolecules* **2002**, *3* (5), 1101–1108. https://doi.org/10.1021/bm020065p.

(28) Lee, J. H.; Lee, J.; Song, K. Bin. Development of a Chicken Feet Protein Film Containing Essential Oils. *Food Hydrocoll.* **2015**, *46*, 208–215. https://doi.org/10.1016/j.foodhyd.2014.12.020.

(29) Yang, H. J.; Lee, J. H.; Won, M.; Song, K. Bin. Antioxidant Activities of Distiller Dried Grains with Solubles as Protein Films Containing Tea Extracts and Their Application in the Packaging of Pork Meat. *Food Chem.* **2016**, *196*, 174–179. https://doi.org/10.1016/j.foodchem.2015.09.020.

(30) Dai, H.; Ou, S.; Huang, Y.; Huang, H. Utilization of Pineapple Peel for Production of Nanocellulose and Film Application. *Cellulose* **2018**, *25* (3), 1743–1756. https://doi.org/10.1007/s10570-018-1671-0.

(31) Gao, C.; Pollet, E.; Avérous, L. Properties of Glycerol-Plasticized Alginate Films Obtained by Thermo-Mechanical Mixing. *Food Hydrocoll.* **2017**, *63*, 414–420. https://doi.org/10.1016/j.foodhyd.2016.09.023.

(32) Han, J. H.; Floros, J. D. Casting Antimicrobial Packaging Films and Measuring Their Physical Properties and Antimicrobial Activity. *J. Plast. Film Sheeting* **1997**, *13* (4), 287–298.

https://doi.org/10.1177/875608799701300405.

(33) Owens, D. K.; Wendt, R. C. Estimation of the Surface Free Energy of Polymers. *J. Appl. Polym. Sci.* **1969**, *13* (8), 1741–1747. https://doi.org/10.1002/app.1969.070130815.

(34) Segal, L.; Creely, J. J.; Martin, A. E.; Conrad, C. M. An Empirical Method for Estimating the Degree of Crystallinity of Native Cellulose Using the X-Ray Diffractometer. *Text. Res. J.* **1959**, *29* (10), 786–794. https://doi.org/10.1177/004051755902901003.

(35) Luo, Y.; Li, X.; Zhang, J.; Liao, C.; Li, X. The Carbon Nanotube Fibers for Optoelectric Conversion and Energy Storage. *J. Nanomater.* **2014**, *2014*, 51–53. https://doi.org/https://doi.org/10.1155/2014/580256.

(36) Liu, P.; Guo, X.; Nan, F.; Duan, Y.; Zhang, J. Modifying Mechanical, Optical Properties and Thermal Processability of Iridescent Cellulose Nanocrystal Films Using Ionic Liquid. *ACS Appl. Mater. Interfaces* **2017**, *9* (3), 3085–3092. https://doi.org/10.1021/acsami.6b12953.

(37) Iwamoto, S.; Nakagaito, A. N.; Yano, H. Nano-Fibrillation of Pulp Fibers for the Processing of Transparent Nanocomposites. *Appl. Phys. A Mater. Sci. Process.* **2007**, *89* (2), 461–466. https://doi.org/10.1007/s00339-007-4175-6.

(38) Murrieta-Martínez, C.; Soto-Valdez, H.; Pacheco-Aguilar, R.; Torres-Arreola, W.; Rodríguez-Felix, F.; Ramírez-Wong, B.; Santacruz-Ortega, H.; Santos-Sauceda, I.; Olibarría-Rodríguez, G.; Márquez-Ríos, E. Effect of Different Polyalcohols as Plasticizers on the Functional Properties of Squid Protein Film (Dosidicus Gigas). *Coatings* **2019**, *9* (2), 77. https://doi.org/10.3390/coatings9020077.

(39) Lee, J. W.; Son, S. M.; Hong, S. I. Characterization of Protein-Coated Polypropylene Films as a Novel Composite Structure for Active Food Packaging Application. *J. Food Eng.* **2008**, *86* (4), 484–493. https://doi.org/10.1016/j.jfoodeng.2007.10.025.

(40) Park, S. Y.; Yook, S.; Goo, S.; Im, W.; Youn, H. J. Preparation of Transparent and Thick CNF/Epoxy Composites by Controlling the Properties of Cellulose Nanofibrils. *Nanomaterials* **2020**, *10* (4), 1–13. https://doi.org/10.3390/nano10040625.

(41) Imran, M.; Revol-Junelles, A. M.; René, N.; Jamshidian, M.; Akhtar, M. J.; Arab-Tehrany, E.; Jacquot, M.; Desobry, S. Microstructure and Physico-Chemical Evaluation of Nano-Emulsion-Based Antimicrobial Peptides Embedded in Bioactive Packaging Films. *Food Hydrocoll.* **2012**, *29* (2), 407–419. https://doi.org/10.1016/j.foodhyd.2012.04.010.

(42) Klangmuang, P.; Sothornvit, R. Barrier Properties, Mechanical Properties and Antimicrobial Activity of Hydroxypropyl Methylcellulose-Based Nanocomposite Films Incorporated with Thai Essential Oils. *Food Hydrocoll.* **2016**, *61*, 609–616. https://doi.org/10.1016/j.foodhyd.2016.06.018.

(43) Tardy, B. L.; Mattos, B. D.; Greca, L. G.; Kämäräinen, T.; Klockars, K. W.; Rojas, O. J. Tessellation of Chiral-Nematic Cellulose Nanocrystal Films by Microtemplating. *Adv. Funct. Mater.* **2019**, *29* (25), 1–12. https://doi.org/10.1002/adfm.201808518.

(44) Baez, C.; Considine, J.; Rowlands, R. Influence of Drying Restraint on Physical and Mechanical Properties of Nanofibrillated Cellulose Films. *Cellulose* **2014**, *21* (1), 347–356. https://doi.org/10.1007/s10570-013-0159-1.

(45) Fillat, A.; Martínez, J.; Valls, C.; Cusola, O.; Roncero, M. B.; Vidal, T.; Valenzuela, S. V; Diaz, P.; Pastor, F. I. J. Bacterial Cellulose for Increasing Barrier Properties of Paper Products. *Cellulose* **2018**, *25* (10), 6093–6105. https://doi.org/10.1007/s10570-018-1967-0.

(46) Ili Balqis, A. M.; Nor Khaizura, M. A. R.; Russly, A. R.; Nur Hanani, Z. A. Effects of Plasticizers on the Physicochemical Properties of Kappa-Carrageenan Films Extracted from Eucheuma Cottonii. *Int. J. Biol. Macromol.* **2017**, *103* (October), 721–732. https://doi.org/10.1016/j.ijbiomac.2017.05.105.

(47) Talja, R. A.; Helén, H.; Roos, Y. H.; Jouppila, K. Effect of Various Polyols and Polyol Contents on Physical and Mechanical Properties of Potato Starch-Based Films. *Carbohydr. Polym.* **2007**, *67* (3), 288–295. https://doi.org/10.1016/j.carbpol.2006.05.019.

(48) Roy, A.; Ghosh, A.; Datta, S.; Das, S.; Mohanraj, P.; Deb, J.; Bhanoji Rao, M. E. Effects of Plasticizers and Surfactants on the Film Forming Properties of Hydroxypropyl Methylcellulose for the Coating of Diclofenac Sodium Tablets. *Saudi Pharm. J.* **2009**, *17* (3), 233–241. https://doi.org/10.1016/j.jsps.2009.08.004.

(49) Deis, R. C.; Kearsley, M. W. Sorbitol and Mannitol. *Sweeten. Sugar Altern. Food Technol.* **2012**, 331–346. https://doi.org/10.1002/9781118373941.ch15.

(50) Santana, A. A.; Kieckbusch, T. G. Physical Evaluation of Biodegradable Films of Calcium Alginate Plasticized with Polyols. *Brazilian J. Chem. Eng.* **2013**, *30* (4), 835–845. https://doi.org/10.1590/S0104-66322013000400015.

(51) Bardet, R.; Belgacem, N.; Bras, J. Flexibility and Color Monitoring of Cellulose Nanocrystal Iridescent Solid Films Using Anionic or Neutral Polymers. *ACS Appl. Mater. Interfaces* **2015**, *7* (7), 4010–4018. https://doi.org/10.1021/am506786t.

(52) Tyagi, P.; Hubbe, M. A.; Lucia, L.; Pal, L. High Performance Nanocellulose-Based Composite Coatings for Oil and Grease Resistance. *Cellulose* **2018**, *25* (6), 3377–3391. https://doi.org/10.1007/s10570-018-1810-7.

(53) Aulin, C.; Gällstedt, M.; Lindström, T. Oxygen and Oil Barrier Properties of Microfibrillated Cellulose

765 Films and Coatings. *Cellulose* **2010**, *17* (3), 559–574. https://doi.org/10.1007/s10570-009-9393-y.
766 (54) Xia, J.; Zhang, Z.; Liu, W.; Li, V. C. F.; Cao, Y.; Zhang, W.; Deng, Y. Highly Transparent 100%
767 Cellulose Nanofibril Films with Extremely High Oxygen Barriers in High Relative Humidity. *Cellulose*
768 **2018**, *25* (7), 4057–4066. https://doi.org/10.1007/s10570-018-1843-y.
769 (55) Sharma, P. R.; Varma, A. J. Thermal Stability of Cellulose and Their Nanoparticles: Effect of
770 Incremental Increases in Carboxyl and Aldehyde Groups. *Carbohydr. Polym.* **2014**, *114*, 339–343.
771 https://doi.org/10.1016/j.carbpol.2014.08.032.
772 (56) Nair, S. S.; Zhu, J.; Deng, Y.; Ragauskas, A. J. High Performance Green Barriers Based on
773 Nanocellulose. *Sustain. Chem. Process.* **2014**, *2* (1), 0–7. https://doi.org/10.1186/s40508-014-0023-0.
774 (57) Wang, J.; Gardner, D. J.; Stark, N. M.; Bousfield, D. W.; Tajvidi, M.; Cai, Z. Moisture and Oxygen
775 Barrier Properties of Cellulose Nanomaterial-Based Films. *ACS Sustain. Chem. Eng.* **2018**, *6* (1), 49–70.
776 https://doi.org/10.1021/acssuschemeng.7b03523.
777 (58) Niskanen, K., F. P. E. A. Papermaking Science and Technology. *Pap. physics. Helsinki* **1998**, *Vol 16*.
778 (59) Zumbé, A.; Lee, A.; Storey, D. Polyols in Confectionery: The Route to Sugar-Free, Reduced Sugar and
779 Reduced Calorie Confectionery. *Br. J. Nutr.* **2001**, *85* (S1), S31–S45.
780 https://doi.org/10.1079/bjn2000260.
781 (60) Zhang, Y.; Han, J. H. Plasticization of Pea Starch Films with Monosaccharides and Polyols. *J. Food Sci.*
782 **2006**, *71* (6), 253–261. https://doi.org/10.1111/j.1750-3841.2006.00075.x.
783 (61) Tong, Q.; Xiao, Q.; Lim, L. T. Effects of Glycerol, Sorbitol, Xylitol and Fructose Plasticisers on
784 Mechanical and Moisture Barrier Properties of Pullulan-Alginate-Carboxymethylcellulose Blend Films.
785 *Int. J. Food Sci. Technol.* **2013**, *48* (4), 870–878. https://doi.org/10.1111/ijfs.12039.
786 (62) Sothornvit, R.; Krochta, J. M. Plasticizer Effect on Mechanical Properties of β-Lactoglobulin Films. *J.*
787 *Food Eng.* **2001**, *50* (3), 149–155. https://doi.org/10.1016/S0260-8774(00)00237-5.
788 (63) Belbekhouche, S.; Bras, J.; Siqueira, G.; Chappey, C.; Lebrun, L.; Khelifi, B.; Marais, S.; Dufresne, A.
789 Water Sorption Behavior and Gas Barrier Properties of Cellulose Whiskers and Microfibrils Films.
790 *Carbohydr. Polym.* **2011**, *83* (4), 1740–1748. https://doi.org/10.1016/j.carbpol.2010.10.036.
791 (64) Gao, Q.; Lei, M.; Zhou, K.; Liu, X.; Wang, S.; Li, H. Preparation of a Microfibrillated
792 Cellulose/Chitosan/Polypyrrole Film for Active Food Packaging. *Prog. Org. Coatings* **2020**, *149*
793 (November 2019), 105907. https://doi.org/10.1016/j.porgcoat.2020.105907.
794 (65) Jung, B. N.; Jung, H. W.; Kang, D. H.; Kim, G. H.; Lee, M.; Shim, J. K.; Hwang, S. W. The Fabrication
795 of Flexible and Oxygen Barrier Cellulose Nanofiber/Polylactic Acid Nanocomposites Using Cosolvent

System. *J. Appl. Polym. Sci.* **2020**, *137* (47), 1–17. https://doi.org/10.1002/app.49536.

(66) Raynaud, S. Development of New Barrier Materials Using Microfibrillated Cellulose To Cite This Version : HAL Id : Tel-01796806 Développement de Nouveaux Matériaux Barrières Utilisant Des Microfibrilles de Cellulose. **2018**.

(67) Sun, X.; Mei, C.; French, A. D.; Lee, S.; Wang, Y.; Wu, Q. Surface Wetting Behavior of Nanocellulose-Based Composite Films. *Cellulose* **2018**, *25* (9), 5071–5087. https://doi.org/10.1007/s10570-018-1927-8.

(68) Nagy, S.; Csiszár, E.; Kun, D.; Koczka, B. Cellulose Nanocrystal/Amino-Aldehyde Biocomposite Films. *Carbohydr. Polym.* **2018**, *194* (January), 51–60. https://doi.org/10.1016/j.carbpol.2018.04.025.

(69) Mujtaba, M.; Salaberria, A. M.; Andres, M. A.; Kaya, M.; Gunyakti, A.; Labidi, J. Utilization of Flax (Linum Usitatissimum) Cellulose Nanocrystals as Reinforcing Material for Chitosan Films. *Int. J. Biol. Macromol.* **2017**, *104*, 944–952. https://doi.org/10.1016/j.ijbiomac.2017.06.127.

(70) Moon, R. J.; Martini, A.; Nairn, J.; Simonsen, J.; Youngblood, J. Cellulose Nanomaterials Review: Structure, Properties and Nanocomposites. *Chem. Soc. Rev.* **2011**, *40* (7), 3941. https://doi.org/10.1039/c0cs00108b.

(71) Brinchi, L.; Cotana, F.; Fortunati, E.; Kenny, J. M. Production of Nanocrystalline Cellulose from Lignocellulosic Biomass: Technology and Applications. *Carbohydr. Polym.* **2013**, *94* (1), 154–169. https://doi.org/10.1016/j.carbpol.2013.01.033.

(72) Islam, N.; Proma, S.; Rahman, A.; Chakraborty, A. Preparation and Biodegradation of Nanocellulose Reinforced Polyvinyl Alcohol Blend Films in Bioenvironmental Media. *Chem. Sci. Int. J.* **2017**, *19* (3), 1–8. https://doi.org/10.9734/csji/2017/32570.

(73) Bagde, P.; Nadanathangam, V. Mechanical, Antibacterial and Biodegradable Properties of Starch Film Containing Bacteriocin Immobilized Crystalline Nanocellulose. *Carbohydr. Polym.* **2019**, *222* (April), 115021. https://doi.org/10.1016/j.carbpol.2019.115021.

(74) Potivara, K.; Phisalaphong, M. Development and Characterization of Bacterial Cellulose Reinforced with Natural Rubber. *Materials (Basel).* **2019**, *12* (14). https://doi.org/10.3390/ma12142323.

(75) Taib, M. N. A. M.; Yehye, W. A.; Julkapli, N. M. Influence of Crosslinking Density on Antioxidant Nanocellulose in Bio-Degradation and Mechanical Properties of Nitrile Rubber Composites. *Fibers Polym.* **2019**, *20* (1), 165–176. https://doi.org/10.1007/s12221-019-8575-y.

(76) Giri, J.; Lach, R.; Grellmann, W.; Susan, M. A. B. H.; Saiter, J. M.; Henning, S.; Katiyar, V.; Adhikari, R. Compostable Composites of Wheat Stalk Micro- and Nanocrystalline Cellulose and Poly(Butylene Adipate-Co-Terephthalate): Surface Properties and Degradation Behavior. *J. Appl. Polym. Sci.* **2019**, *136*

(43), 1–11. https://doi.org/10.1002/app.48149.

(77) Gatidou, G.; Vazaiou, N.; Thomaidis, N. S.; Stasinakis, A. S. Biodegradability Assessment of Food Additives Using OECD 301F Respirometric Test. *Chemosphere* **2020**, *241*, 125071. https://doi.org/10.1016/j.chemosphere.2019.125071.

(78) Hall, M.; Bansal, P.; Lee, J. H.; Realff, M. J.; Bommarius, A. S. Cellulose Crystallinity - A Key Predictor of the Enzymatic Hydrolysis Rate. *FEBS J.* **2010**, *277* (6), 1571–1582. https://doi.org/10.1111/j.1742-4658.2010.07585.x.

FIGURES

- **Fig. 1**. Transparency [a), as calculated from eq. 2] and specular gloss [b)] of CNC-based films containing additives at a dose of 10 or 25% as compared to the additive-free control film (line).
- **Fig. 2**. Tensile strength [a)], Elongation at break [b)] and Young-modulus [c)] of the control film (line) and films containing an additive (columns).
- **Fig. 3.** Effect of the type of plasticizer and its dose on roughness (%) relative to the control film (line).
- **Fig. 4.** Scanning electron micrographs of the control film (a and b) and others containing an additive (c and d).
- **Fig. 5.** Air permeance (µm Pa^{-1} s^{-1}) of the CNC-based films, at different doses of additives.
- **Fig. 6.** WDT (min) of the CNC-control film (line) and CNC-based films additives (columns).
- **Fig. 7.** Contact angle (°) of the control film (line- with a confidence interval of ± 0.10) and the films containing additives (columns).
- **Fig. 8.** Water vapor transmission rate (WVTR) a) at 50% RH and theoretical porosity, b) at 90% RH and the OH group content.
- **Fig. 9.** Oxygen permeability (OP) of control and additive-containing films (Sor, Gly, Mal and Xyl).
- **Fig. 10.** Oxygen permeability (OP) at 80% RH and water vapor transmission rate (WVTR) at 50% RH of control and additive-containing films (Sor, Gly, Mal and Xyl).
- **Fig. 11.** Surface free energy (SFE) of the control film (CNC) and additive-containing films.
- **Fig. 12.** Polar component and OH number of the additive-containing films.
- **Fig. 13.** FTIR spectra for the control and additive-containing films.

- **Fig. 14.** XRD patterns for the control film and others containing Sor, Xyl, Man or Gg at a 25% dose.
- **Fig. 15.** Biodegradability, measured in accumulated CO_2 over time, of the films with the different additives added in 25%, as well as the control.

SUPPORTING INFORMATION

- **Fig. S1**. Orthogonal (A) and oblique projection (B) of an additive-free film (*a*) and others containing the following plasticizers: (*b*) Sor, (*c*) Gly, (*d*) Mal, (*e*) Xyl, (*f*) Man, (*g*) Gg and (*h*) Eg.
- **Fig. S2.** Absorbance curves for the films containing an additive at a 25% dose.
- **Fig. S3.** Tensile strength [a)], Elongation at break [b)] and Young-modulus [c)] of the control film (line) and others containing an additive.
- **Fig. S4**. Optical micrographs of the control (a) film and others containing one of the different additives at a 25% dose: Sor (b), Gly (c), Mal (d), Xyl (e), Man (f), Gg (g) and Eg (h).
- **Fig. S5**. FTIR spectra of the additives.
- **Fig. S6.** FTIR spectra of the additives, control, and additive-containing films.
- **Table S1**

  Chemical structure, OH number and molecular weight of additives.
- **Table S2**

  Mechanical properties of the CNC films.
- **Table S3**

  Basis weight, thickness and apparent density of the films.
- **Table S4**

  Crystallinity index (CI) as calculated from eq.4 of CNC films containing no additive (control), or a 25% dose of Sor, Xyl, Man or Gg.

Video "Oil_resistance" about the methodology performed to carry out this essay

FIGURE 1

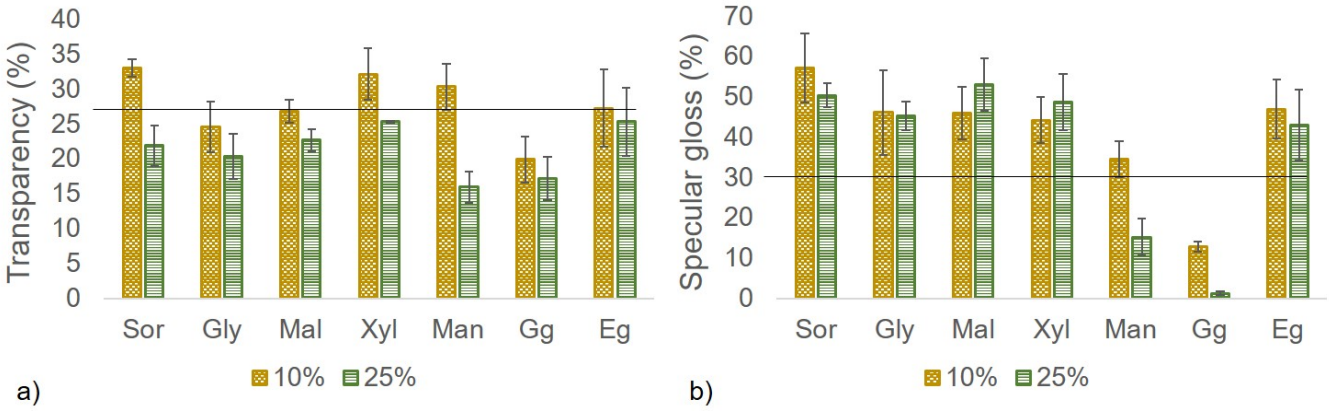
Transparency (%)
40
35
30
25
20
15
10
5
0
Sor
Gly
Mal
Xyl
Man
Gg
Eg
10%
25%
a)
Specular gloss (%)
70
60
50
40
30
20
10
0
Sor
Gly
Mal
Xyl
Man
Gg
Eg
10%
25%
b)

FIGURE 2

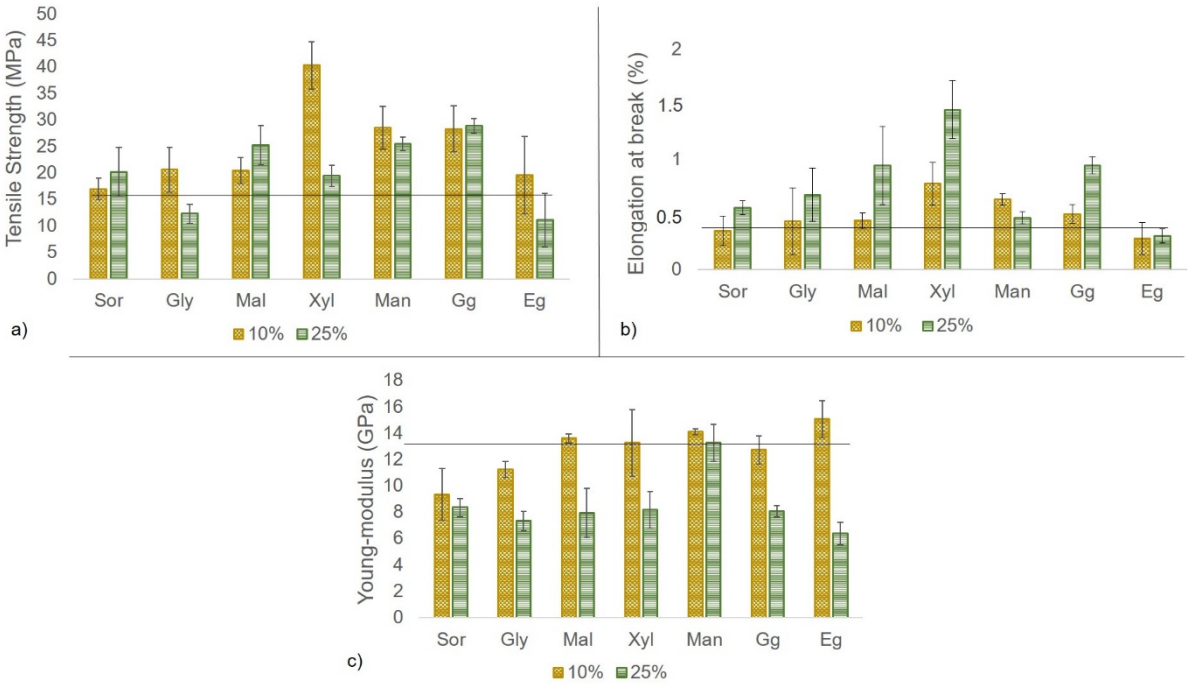
Tensile Strength (MPa)
50
45
40
35
30
25
20
15
10
5
0
Sor
Gly
Mal
Xyl
Man
Gg
Eg
10%
25%
a)
Elongation at break (%)
2
1.5
1
0.5
0
Sor
Gly
Mal
Xyl
Man
Gg
Eg
10%
25%
b)
Young-modulus (GPa)
18
16
14
12
10
8
6
4
2
0
Sor
Gly
Mal
Xyl
Man
Gg
Eg
10%
25%
c)

FIGURE 3

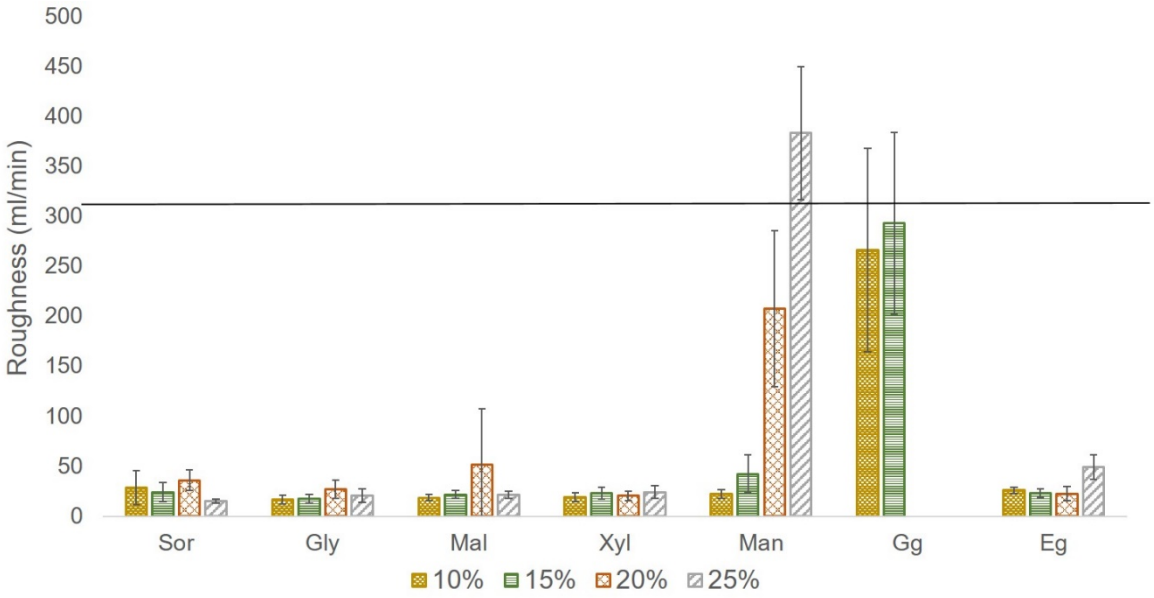
Roughness (ml/min)
500
450
400
350
300
250
200
150
100
50
0
Sor
Gly
Mal
Xyl
Man
Gg
Eg
10%
15%
20%
25%

FIGURE 4

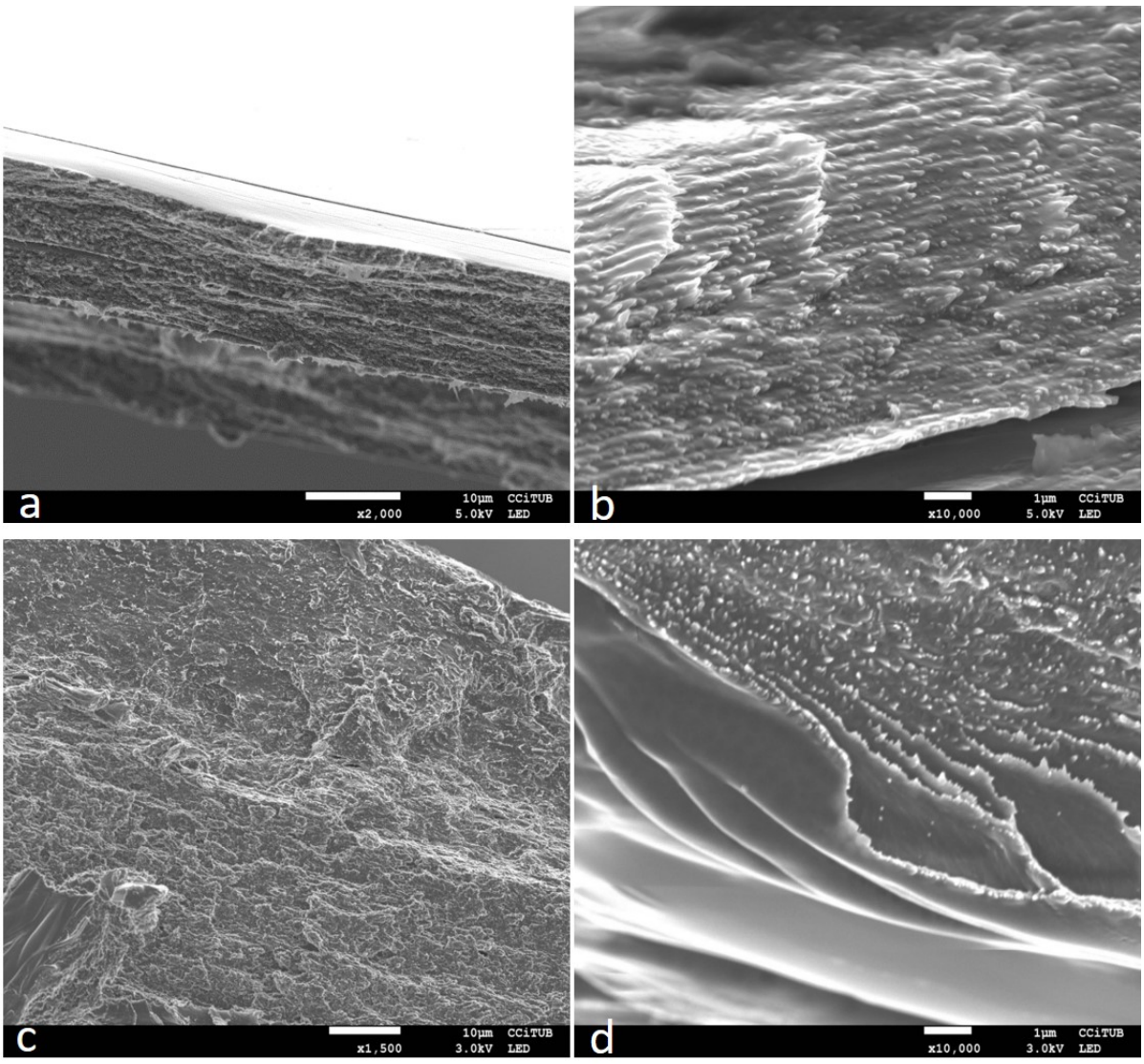
a
10µm CCiTUB
x2,000 5.0kV LED
b
1µm CCiTUB
x10,000 5.0kV LED
c
10µm CCiTUB
x1,500 3.0kV LED
d
1µm CCiTUB
x10,000 3.0kV LED

FIGURE 5

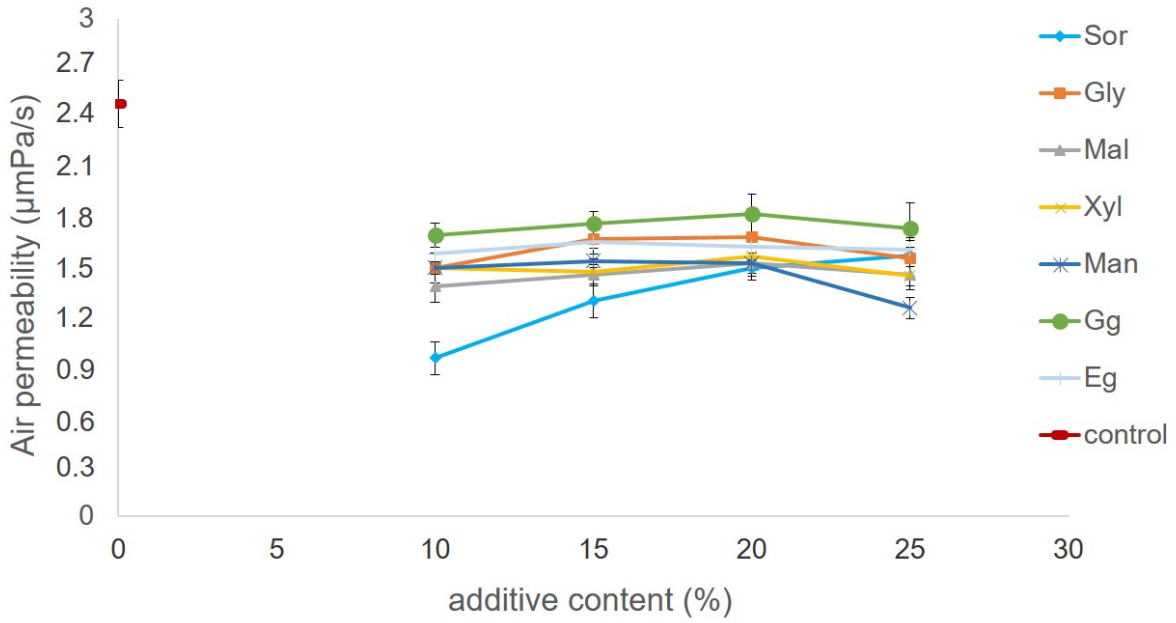
Air permeability (µmPa/s)
3
2.7
2.4
2.1
1.8
1.5
1.2
0.9
0.6
0.3
0
0
5
10
15
20
25
30
additive content (%)
Sor
Gly
Mal
Xyl
Man
Gg
Eg
control

FIGURE 6

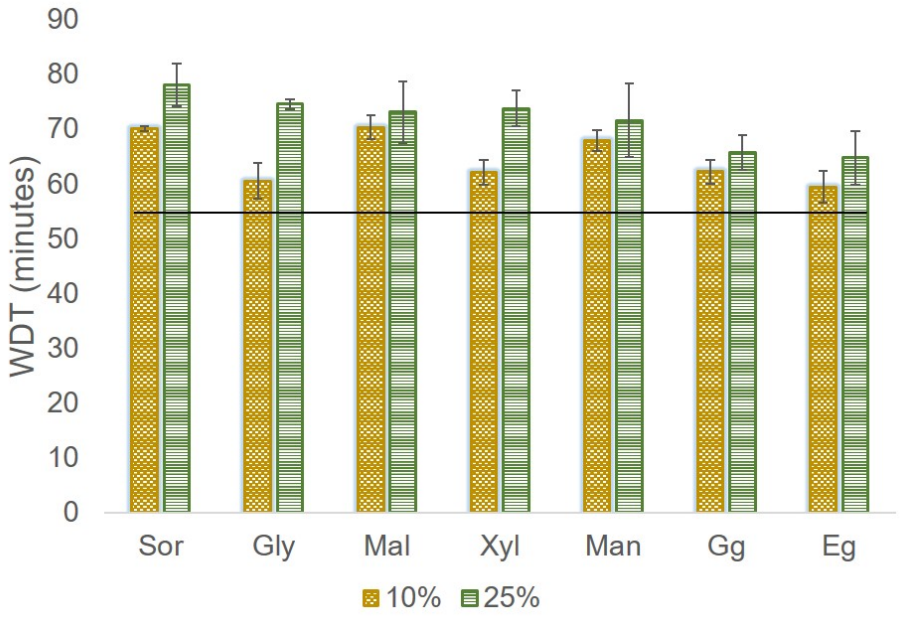
90
80
70
60
50
40
30
20
10
0
WDT (minutes)
Sor
Gly
Mal
Xyl
Man
Gg
Eg
10%
25%

FIGURE 7

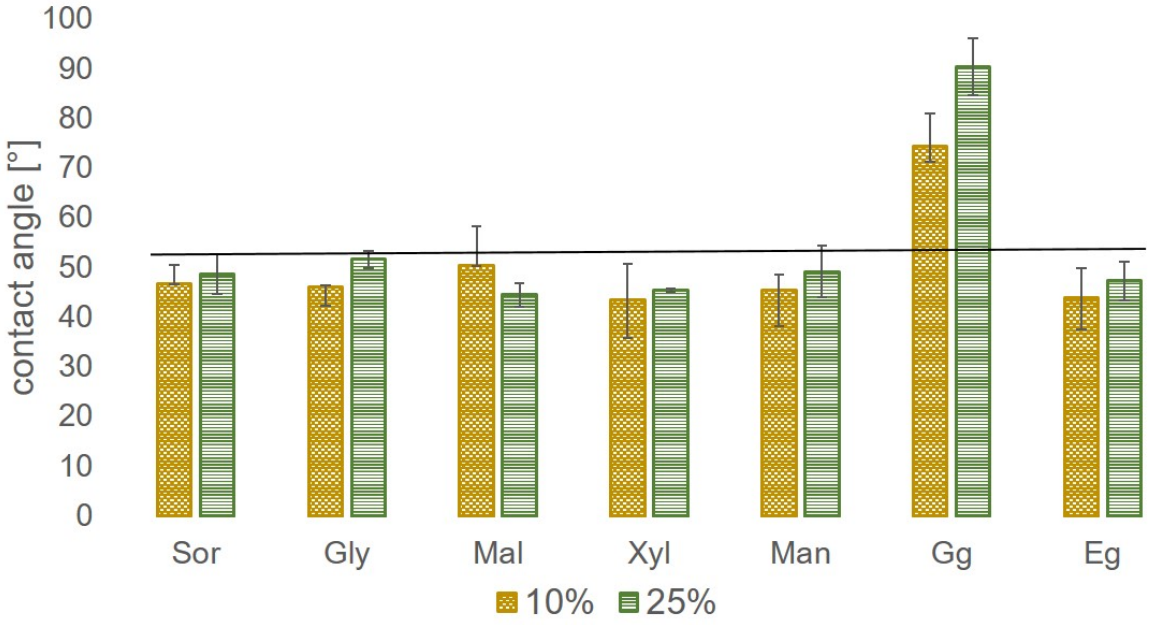
100
90
80
70
60
50
40
30
20
10
0
contact angle [°]
Sor
Gly
Mal
Xyl
Man
Gg
Eg
10%
25%

FIGURE 8

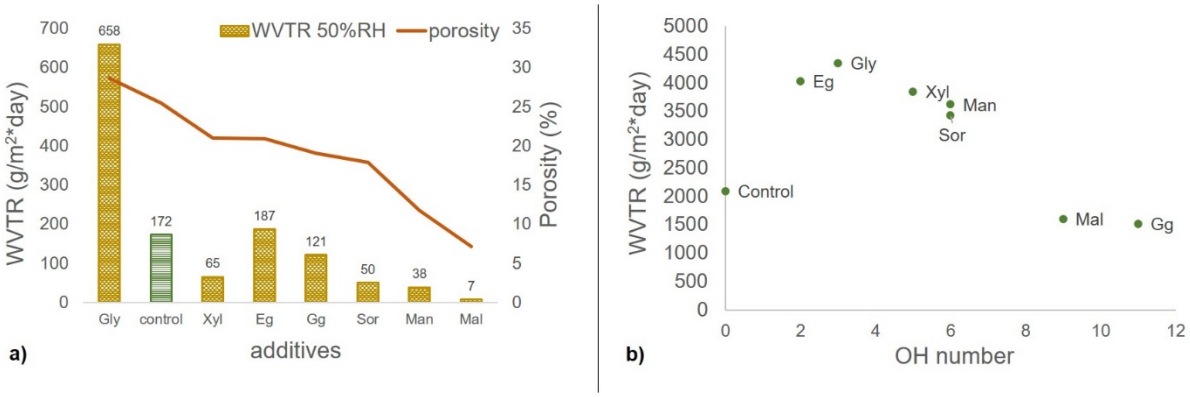
WVTR 50%RH
porosity
WVTR (g/m²*day)
Porosity (%)
658
172
65
187
121
50
38
7
Gly
control
Xyl
Eg
Gg
Sor
Man
Mal
additives
a)
Gly
Eg
Xyl
Man
Sor
Control
Mal
Gg
OH number
b)

FIGURE 9

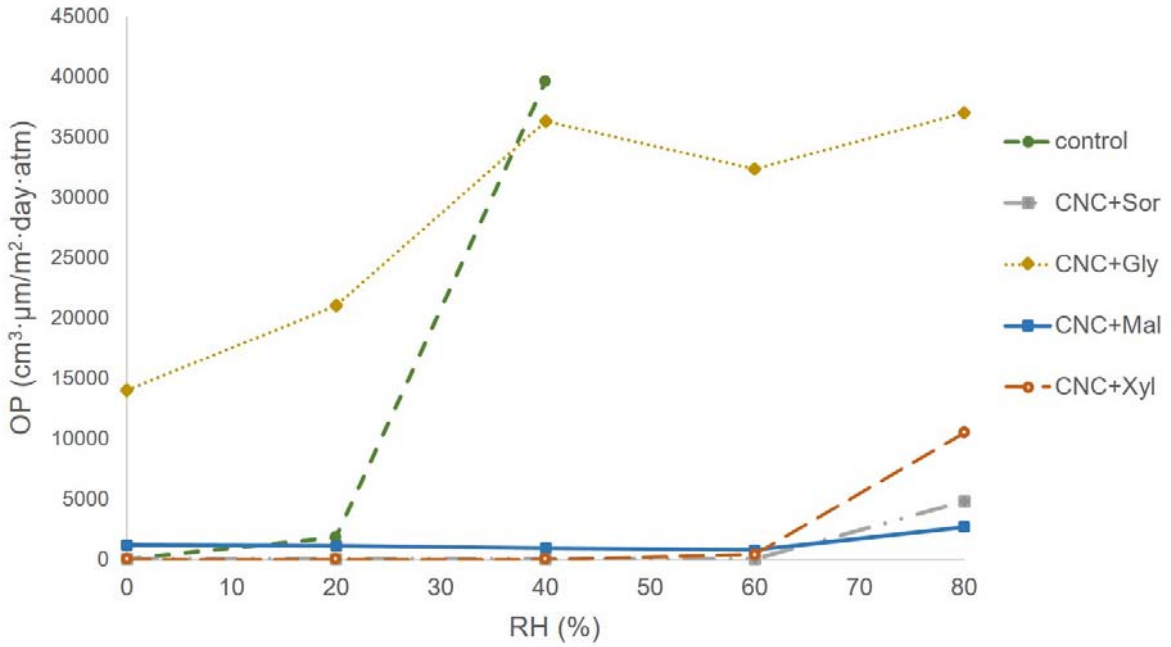
45000
40000
35000
30000
25000
20000
15000
10000
5000
0
OP (cm³·µm/m²·day·atm)
0
10
20
30
40
50
60
70
80
RH (%)
control
CNC+Sor
CNC+Gly
CNC+Mal
CNC+Xyl

FIGURE 10

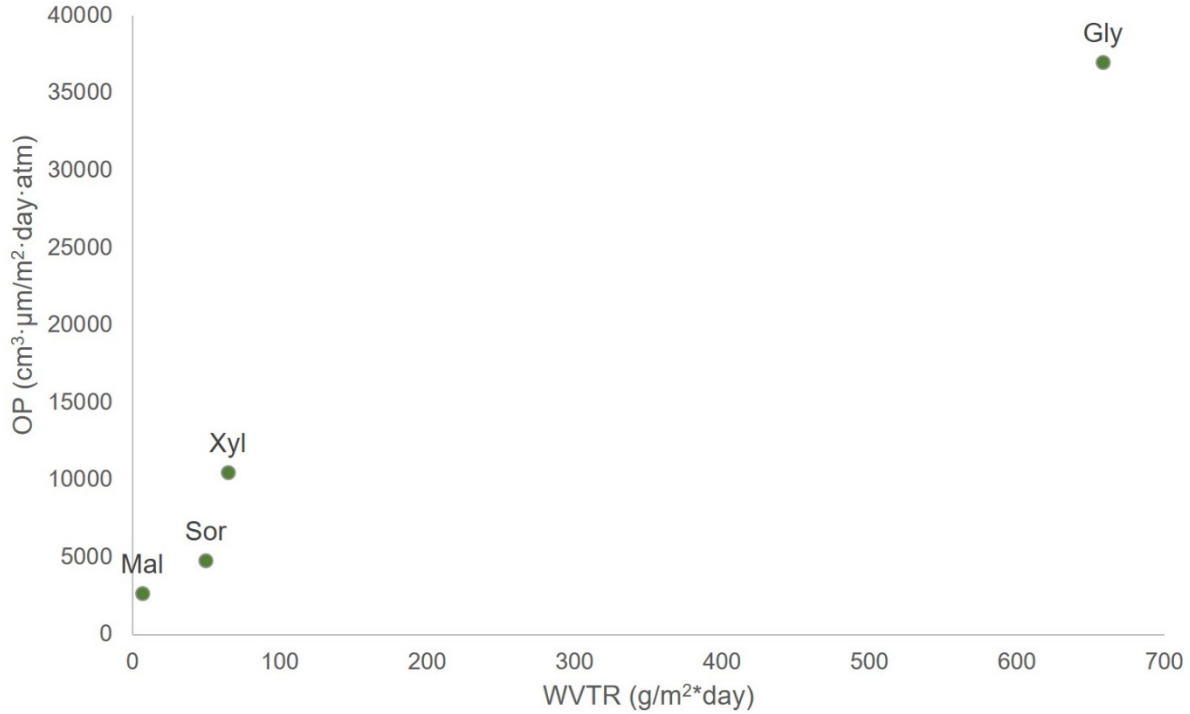
40000
35000
30000
25000
20000
15000
10000
5000
0
OP (cm³·µm/m²·day·atm)
Gly
Xyl
Sor
Mal
0
100
200
300
400
500
600
700
WVTR (g/m²*day)

FIGURE 11

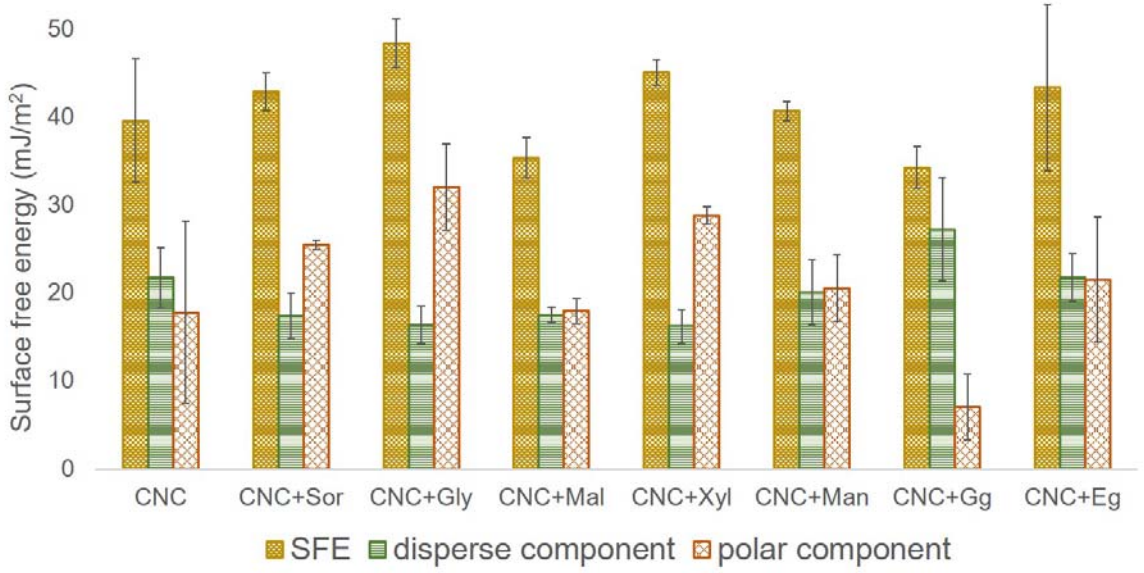
Surface free energy (mJ/m²)
50
40
30
20
10
0
CNC
CNC+Sor
CNC+Gly
CNC+Mal
CNC+Xyl
CNC+Man
CNC+Gg
CNC+Eg
SFE
disperse component
polar component

FIGURE 12

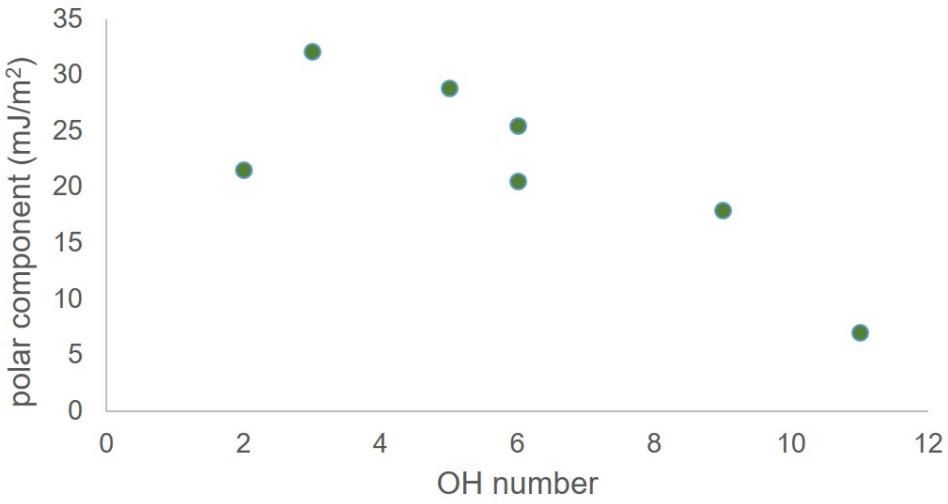

FIGURE 13

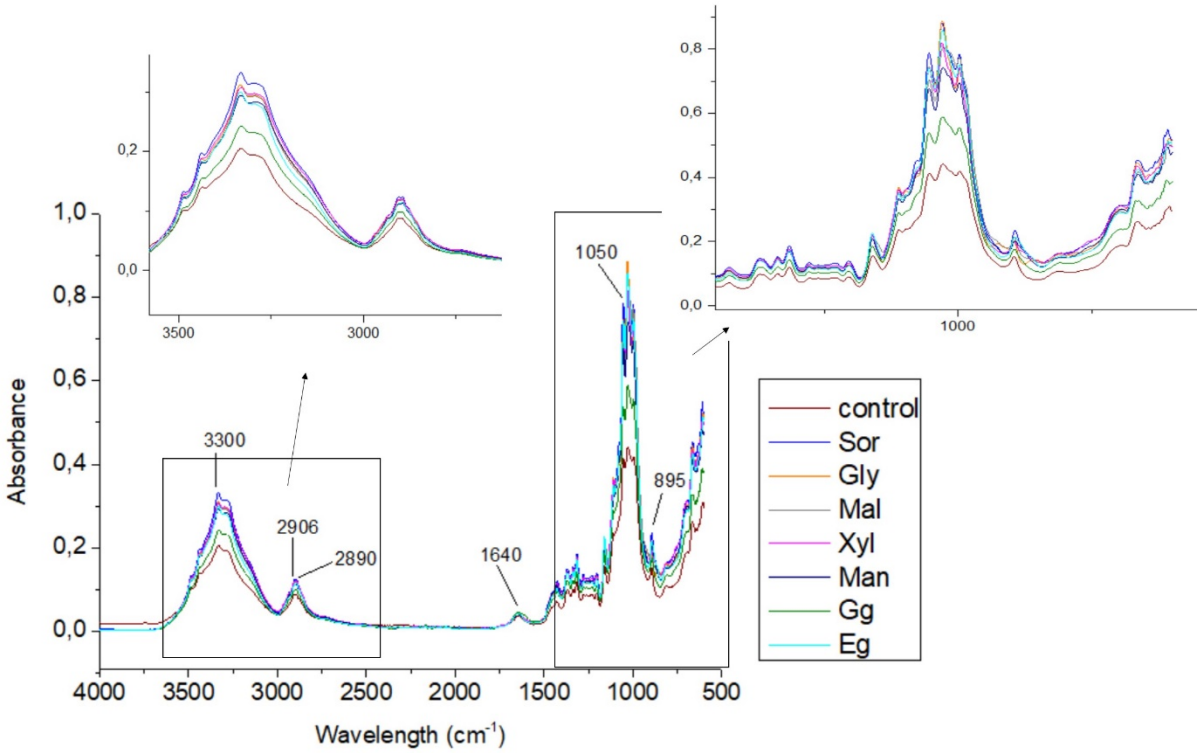
Absorbance
Wavelength (cm-1)
3300
2906
2890
1640
1050
895
control
Sor
Gly
Mal
Xyl
Man
Gg
Eg

FIGURE 14

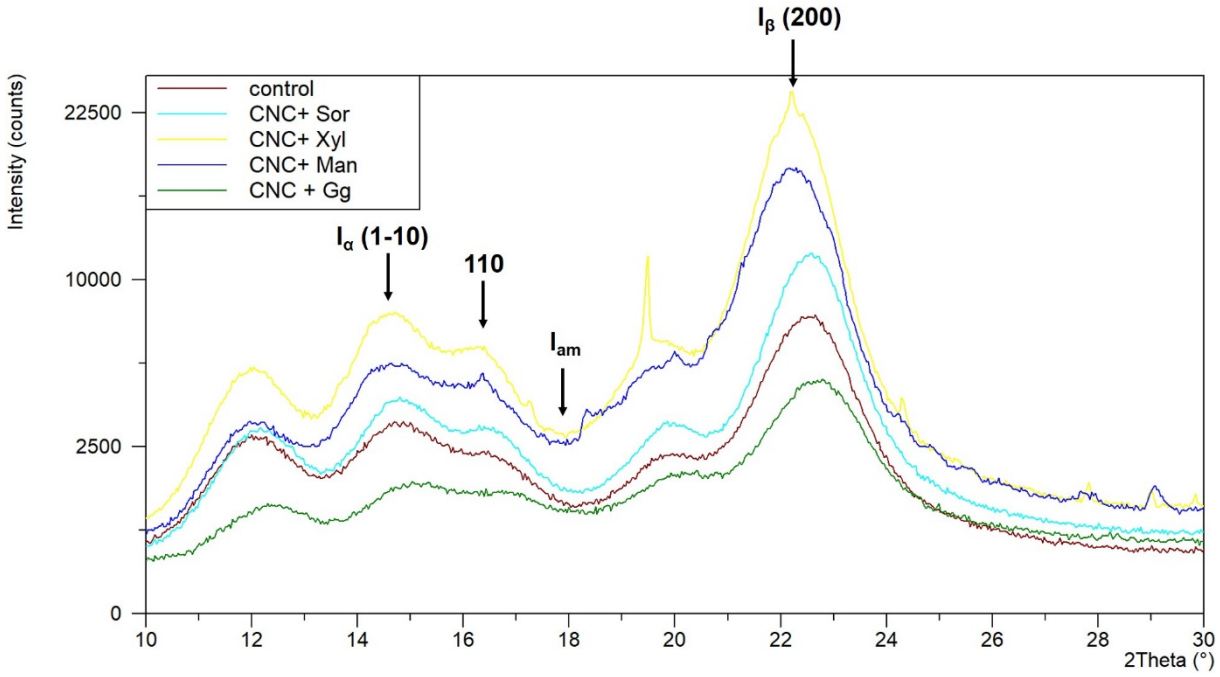
Iβ (200)
control
CNC+ Sor
CNC+ Xyl
CNC+ Man
CNC + Gg
Intensity (counts)
22500
10000
2500
0
Iα (1-10)
110
Iam
10
12
14
16
18
20
22
24
26
28
30
2Theta (°)

FIGURE 15

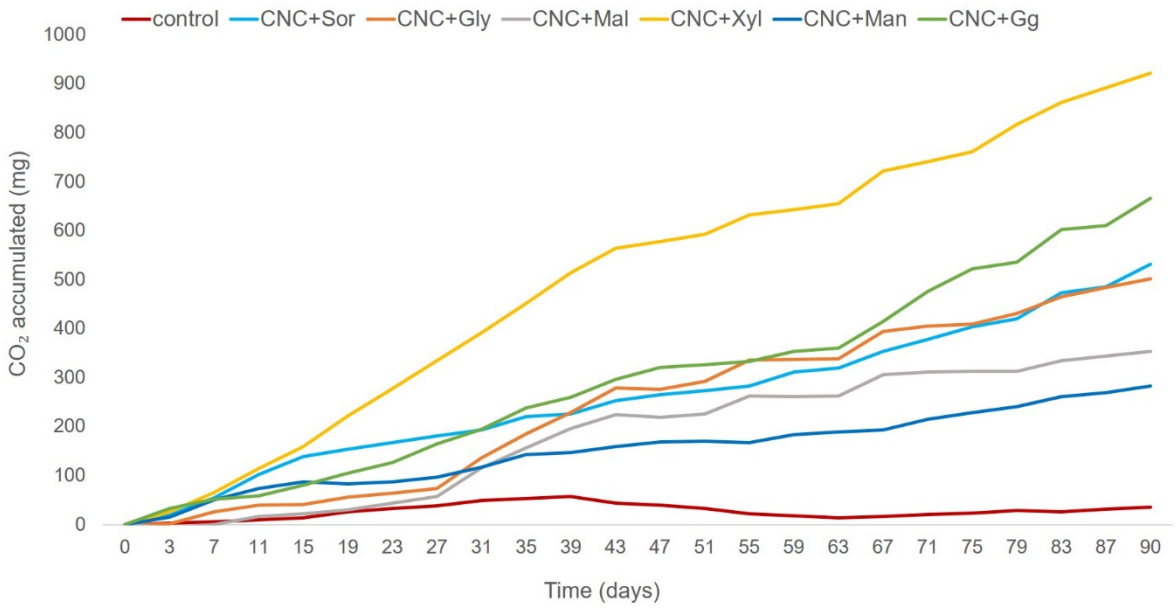
control
CNC+Sor
CNC+Gly
CNC+Mal
CNC+Xyl
CNC+Man
CNC+Gg
CO_2 accumulated (mg)
1000
900
800
700
600
500
400
300
200
100
0
0 3 7 11 15 19 23 27 31 35 39 43 47 51 55 59 63 67 71 75 79 83 87 90
Time (days)

FOR TABLE OF CONTENTS USE ONLY

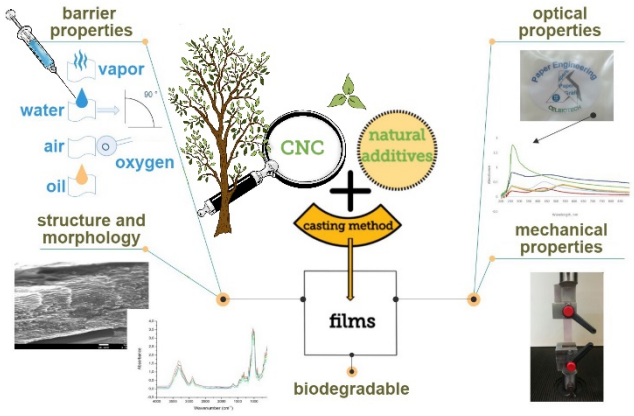

Abstract Graphics. Obtaining sustainable, biobased and biodegradable CNC-based films with natural additives. Evaluation of barrier, mechanical, optical, structural properties, and morphology.